https://doi.org/10.5194/essd-2026-839
Preprint. Discussion started: 11 November 2026
© Author(s) 2026. CC BY 4.0 License.



Open Access Earth System Science Data Discussions

High-Elevation Meteorological Datasets from the Quelccaya Ice Cap and Surrounding Sites in the Cordillera Vilcanota, Peru: 2012-2026

L. Baker Perry[1,2], Arbindra Khadka[3], Ludving Cano[1], Anton Seimon[1,4], Tom Matthews[5], Sandro Arias[6], Heather Guy[7,8], Maxwell Rado[9], Nilton Montoya[9], Courtney Cooper[10], Wilson Suarez[6]

[1]University of Nevada, Reno, Reno, NV, USA
[2]Appalachian State University, Boone, NC, USA
[3]Tribhuvan University, Kathmandu, Nepal
[4]Bard College, Annandale-on-Hudson, NY, USA
[5]King's College London, London, UK
[6]Servicio Nacional de Meteorología e Hidrología (SENAMHI), Lima, Peru
[7]University of Leeds, Leeds, UK
[8]National Centre for Atmospheric Science, Leeds, UK
[9]Universidad Nacional de San Antonio de Abád del Cusco (UNSAAC), Cusco, Peru
[10]Berry College, Mount Berry, GA, USA

Correspondence to: Arbindra Khadka (arikhadka@gmail.com)

Abstract. The Cordillera Vilcanota of Peru, the second largest glacierized mountain range in the tropics and home to the Quelccaya Ice Cap, is a critical water tower that has experienced rapid glacier retreat and environmental change in recent decades. Here, we present quality-controlled meteorological datasets (between 2012 and 2026) from five automatic weather stations (AWSs) spanning elevations from 4,895 to 6,349 m: Lake Sibinacocha (4,895 m), Murmurani Alto (5,050 m), Osjollo Anante (5,540 m), Quelccaya Ice Cap (5,650 m), and Ausangate (6,349 m). Available variables include temperature, relative humidity, wind speed, wind direction, barometric pressure, snow height change, and solar irradiance. Precipitation amount and type are also available from Lake Sibinacocha and Quelccaya Ice Cap AWSs, while selected snow pit observations and radiosonde data from upper-air soundings complement the surface meteorological observations. The datasets have direct relevance to investigations on topics such as precipitation characteristics, climate-cryosphere interactions, environmental change, and paleoclimatic reconstructions from ice, peat, and sediment cores. All datasets are publicly available at https://doi.org/10.5281/zenodo.23315967 (Perry et al., 2026).

1. Introduction

High-elevation mountain regions are critical global water towers that sustain over a billion people downstream (Immerzeel et al., 2020), but are experiencing widespread climate impacts due to dynamical (e.g., atmospheric circulation and storm tracks) and thermodynamical (e.g., warming and moistening) processes. Resulting impacts include cryospheric melting, more intense

https://doi.org/10.5194/essd-2026-839
Preprint. Discussion started: 11 November 2026
© Author(s) 2026. CC BY 4.0 License.



precipitation, and a higher percentage of total precipitation falling as rain. Destabilization of glaciers and mountain slopes, combined with more frequent and intense liquid precipitation (rain) at the highest elevations, has increased the risk of glacier lake outburst flood events (e.g., Emmer et al., 2025) and landslides (Zou et al., 2026). The 26 August 2026 Bhote Koshi landslide, glacier collapse, and catastrophic flood was but one recent example of the increasing elevation-dependent hazards in mountain regions (Richter 2026). More broadly, the well-documented increase in heavy precipitation and rain-on-snow events has magnified the risk of catastrophic river flooding in mountain regions (e.g., Roohi et al., 2025; Musselman et al., 2018). However, the magnitude of these changes and associated physical processes remain severely understudied largely due to a lack of in situ observational networks at the highest elevations, where most glacier ice and snow occur (Matthews et al., 2020a).

Globally, only a handful of automatic weather station (AWS) networks extend into the critical glacier accumulation zone in the world's highest mountains across the Andes and Hindu Kush Himalaya ranges (e.g., Khadka et al., 2026, Pitte et al., 2026, Matthews et al., 2020a). High-quality observations from weighing precipitation gauges surrounded by properly shielded single or double alter shields are notably lacking at the highest elevations (e.g., Perry et al., 2020), leaving big gaps in understanding of the accumulation processes on glacier surfaces and in the overall hydrological cycle. Until recent installations (e.g., Pitte et al., 2026, Matthews et al., 2020a, Perry et al., 2017), there have been no AWSs that explicitly measure liquid equivalent (LE) precipitation in the accumulation zone in tropical or subtropical high-elevation mountain regions (Condom et al., 2020).

The Andean cordilleras in Ecuador, Peru and Bolivia are home to ~95% of all glaciers in the tropics (23.5°N to 23.5°S latitude; Rabatel et al., 2013). They serve as vital water resources and crucial indicators for assessing the rate and magnitude of past and current climate change (Thompson et al., 2021). They are currently undergoing rapid retreat, with a loss of 42% in areal extent between 1990 and 2020 (Turpo Cayo et al., 2022), yet no long-term (>10 years) AWS networks exist that encompass elevations >5,500 m into the accumulation zone. One of the earliest networks was from the Quelccaya Ice Cap Stations near the summits of Bolivia's Nevado Sajama (6,515 m; Hardy et al., 1998) and Nevado Illimani (6,350 m; Wagnon et al., 2003, Hardy et al., 1998) were the highest in the world at the time and recorded intermittent data between 1996 and 2002. Observations from the Chacaltaya Observatory (5,240 m) in the Cordillera Real of Bolivia provided unprecedented insight into the processes that drove the demise and ultimate disappearance of the Chacaltaya glacier (Francou et al., 2003). Although Chacaltaya is the highest station in the WMO Global Atmospheric Watch (GAW) network (Andrade and Laj 2026), it no longer extends into the glacier accumulation zone and only has high-quality precipitation observations since 2014 (Perry et al., 2017).

The Cordillera Vilcanota in southern Peru has the second largest glacierized area in the tropics (Seimon et al., 2017, Davies et al., 2026), numerous peatlands (*bofedales*; e.g. Gribbin et al., 2024, Perez & Loisel 2023) and serves as the source of the Vilcanota-Urubamba River that provides hydropower and freshwater resources to regions downstream. The Cordillera Vilcanota is a recognized hotspot for Andes-Amazon hydroclimatic connectivity (Espinoza et al., 2015), with >90% of the 72-hr backward air trajectories tied to precipitation events originating over the Amazon Basin (Perry et al., 2014, 2017). The

https://doi.org/10.5194/essd-2026-839
Preprint. Discussion started: 11 November 2026
© Author(s) 2026. CC BY 4.0 License.


impacts of Amazon deforestation and land use change on the hydrological cycle and precipitation delivery mechanisms in the Cordillera Vilcanota and adjacent cordilleras on the northern and eastern edge of the Altiplano are likewise well established (e.g., Sierra et al., 2022), adding to the urgency and importance of the establishment and operation of long-term observational networks in the region.

The Cordillera Vilcanota is also home to the Quelccaya Ice Cap, the second largest tropical glacier and one of the few annually resolvable paleoclimatic archives in the tropics and subtropics, that has led to transformative understanding of tropical and global climate change (Thompson et al., 1985, 2013, 2017, 2021). Early AWSs provided intermittent observations of temperature and net radiation between 1976 and 1978 (Thomspon et al., 1979). Yet, despite its importance and rapid loss in total glacier area (-37%) between 1985 and 2022 (Lamantia et al., 2024), no long-term weather station data exist before 2004, when the University of Massachusetts (UMASS, USA) installed a station at the summit of the Quelccaya Ice Cap (5,680 m; Yarleque et al., 2018). A high-quality record of temperature and snow height change between 2004 and 2017 now exists (Hurley et al., 2019), but the AWS did not include precipitation sensors and other meteorological data have not yet been published.

Through a partnership among the Universidad Nacional de San Antonio Abad del Cusco (UNSAAC, Peru), Appalachian State University (App State, USA), the Peruvian National Hydrology and Meteorology Service (SENAMHI), and local community members, in 2012 our team began installation of a network of five AWSs in the Cordillera Vilcanota at elevations ranging from 4,895 m to 6,349 m, with a particular emphasis on high-quality observations of precipitation and precipitation type (Perry et al., 2017). Although the data have been critical in testing hypotheses related to precipitation characteristics and moisture source regions (e.g., Perry et al., 2017, 2014), ENSO-precipitation relationships (Jonaitis et al., 2021), and meteorological controls on stable water isotopes of oxygen and deuterium (Guy et al., 2019), the comprehensive datasets have not yet been introduced and made publicly available. Researchers in other fields may find the data of use to investigate climate-cryosophere interactions, environmental change, and paleoclimatic reconstructions from ice, peat, and sediment cores.

The aims of this paper are to summarize (1) the site selection and installation of five high-elevation AWSs operated in the Cordillera Vilcanota since 2012; (2) present initial climatologies and known data quality issues from the available data; (3) compare co-located snow pit and precipitation observations from the Quelccaya Ice Cap, and (4) provide direct comparisons between the in situ precipitation observations and ERA5 and ERA5 Land reanalysis datasets. Since reanalysis datasets such as ERA5 and ERA5 Land (Hersbach et al., 2020) are widely used in high-elevation mountain regions (e.g., Khanal et al., 2023, Khadka et al., 2022, Birkel et al., 2022, Matthews et al., 2020b), it is important to validate them against high-quality in situ observations where available.

https://doi.org/10.5194/essd-2026-839
Preprint. Discussion started: 11 November 2026
© Author(s) 2026. CC BY 4.0 License.



2. Dataset descriptions

2.1. Station installations and site characteristics

The station sites, elevations and periods of record are as follows: Murmurani Alto (5,050 m; 2012-2017), Osjollo Anante (5,540 m; 2012-2015), Quelccaya Ice Cap (5,650 m; 2014-2026), Laguna Sibinacocha (4,895 m; 2017-2026), and Nevado Ausangate (6,349 m; 2022). Table 1 summarizes the station elevations, locations, data completeness, time periods, sensors, and geomorphic environment. Station locations, photos, and corresponding ERA5 and ERA5 Land grids (Fig. 1) provide additional metadata and site contexts.

The first site was installed at Murmurani Alto (5,050 m) in April 2012. It was located on a small island in a *bofedal* (peat bog) and included a standard tripod with measurements of temperature, relative humidity, solar irradiance, pressure, soil moisture and temperature, snow depth, and the precipitation type and intensity from a Parsivel disdrometer. The installation on the nearby icecap of Osjollo Anante AWS (5,540 m) was completed only a few days after the installation of the Murmurani Alto AWS. We completed annual visits to download data and raise the station in 2013 and 2014. The station was removed in July 2015 due to the growing risk of crevasses and imminent collapse of the access ramp.

Installation of the Quelccaya Ice Cap AWS (5,650 m) began in August 2014 and was finalized in October 2014. To minimize the effects of ice cap topographic characteristics on firn and ice movement and on precipitation measurement, we selected the flattest location with the highest elevation possible, approximately 30 m lower and 0.5 km WSW from the summit. Access to the site required a ~5 km low-angled ascent of ~300 m with minimal crevasse or avalanche hazard. The station was designed to allow for the ~2 m net annual accumulation (Hurley et al., 2015) and a Belfort double alter shield was installed around the weighing precipitation gauge to minimize precipitation undercatch due to wind (e.g., Kochendorfer et al., 2018, Rasmussen et al., 2012, Goodison et al., 1998). Due to the high frequency of lightning and risk of damage to the station and sensors, four lightning arrestors were installed on vertical alter shield supports. The station and sensors were raised 2 m in 2015, 2017, 2018, 2019, 2021, and 2025; raises of only 1 m were needed in 2023 and 2025. No raise was needed in 2016 due to 14 cm net ablation. The full maintenance history and associated photos are available in metadata.

The Murmurani Alto AWS was decommissioned and moved to Lake Sibinacocha Dam (4,895 m) in July 2017 to provide easier long-term access and security, and to allow for the addition of an OTT HydroMet Pluvio^2 weighing precipitation gauge surrounded by a single alter shield. The AWS is on the southern end of the 16 km long Lake Sibinacocha and is co-located with a conventional AWS operated by SENAMHI Peru (47E8B578).

The Ausangate station (6,349 m) was installed on a broad ice field near the south summit, approximately 35 m below the main summit, as part of the National Geographic and Rolex Perpetual Planet expedition in July 2022. The station was built by Hoskin Scientific (Canada) and modeled after an AWS installed near the summit of Mount Logan, Canada (Holland et al., 2026). In addition to standard meteorological sensors of temperature, relative humidity, pressure, and wind speed and direction, it included both incoming and outgoing radiation and snow depth.

https://doi.org/10.5194/essd-2026-839
Preprint. Discussion started: 11 November 2026
© Author(s) 2026. CC BY 4.0 License.



Snow density and snow water equivalent (SWE) observations from snow pits dug adjacent to the Osjollo Anante, Quelccaya, and Ausangate AWSs complemented the AWS data during annual maintenance visits. Samples from some of the snow pits were also analyzed for water isotopes ($\delta^{18}O$, $\delta^{2}H$) as outlined in Guy et al. (2019). Our teams released radiosondes (weather balloons) during field campaigns in the Cordillera Vilcanota in November 2014 and March 2018. All releases were between Nevado Ausangate and the Quelccaya Ice Cap (Fig. 1).

Although the AWSs were installed at different times and have different variables, T, RH, and snow depth are common across all stations. Given the high power requirements and potential for failure of the electronics and fans in mechanically ventilated radiation shields, coupled with our primary focus on precipitation processes, we opted to use only naturally ventilated radiation shields at our stations. A well-known positive bias in temperature (e.g., Matthews et al., 2020a, Georges & Kaser 2002) exists for naturally ventilated radiation shields in full sunshine, high-albedo fresh snow, and calm winds, so users should treat absolute maximum values on these days with caution. Additional details on station instrumentation, maintenance, and data quality control are provided in the linked Supplement and Metadata. To provide direct comparison along an elevation transect, we also analyzed meteorological data between Murmurani and Osjollo Anante for April 2012 to March 2015, similarly between Quelccaya and Sibinacocha for April 2018-March 2021, as they have the longest overlapping period and 490 to 755 m vertical separation (Figs. S1-S7; Tables S1-S3).

2.2. Radiosondes

Our teams released 18 i-Met-1 radiosondes during field campaigns in the Cordillera Vilcanota in November 2014 and March 2018 using an i-MET 3050 mobile sounding base station. Raw, unprocessed data files include measurements of pressure, temperature, relative humidity with respect to water, and GPS-derived wind speed and direction. Release locations included (a) Quisoquipina Base Camp (5,150 m) at 1200 UTC on 4 November 2014; (b) Quelccaya Base Camp (4,950 m) at 1800 UTC on 4 November 2014, 0000 UTC on 5 November 2014, and 0000 and 1200 UTC on 6 November 2014; (c) Universidad Nacional de San Antonio de Abád del Cusco (UNSAAC) campus (3,365 m) at 2100 UTC on 7 November 2014, 1800 UTC on 8 March 2018, 0000 UTC and 1800 UTC on 9 March 2018, and 0000 and 1800 UTC on 10 March 2018; (d) Chillca (4,350 m) at 0000 and 0600 UTC on 4 March 20218; and (e) Phinaya (4,715 m) at 1800 UTC on 4 March 2018, 0100 and 1900 UTC on 5 March 2018, 0000 UTC on 6 March 2018, and 0000 UTC on 7 March 2018. Users should be aware of documented errors in radiosonde temperature and relative humidity measurements (e.g., Ferreira et al. 2026). Manufacturer-quoted accuracies are ±0.3°C for temperature, ±5% for relative humidity, ±1.8 hPa (> 400 hPa) and ±0.5 hPa (<400 hPa) for pressure, and ±0.06 m s^{-1} for wind speed. i-Met-1 radiosonde temperature data were within 0.5°C of Vaisala RS92 radiosondes during 28 flights as part of the MOHAVE-2009 field campaign (Hurst et al. 2011).

https://doi.org/10.5194/essd-2026-839
Preprint. Discussion started: 11 November 2026
© Author(s) 2026. CC BY 4.0 License.



165 ***Table 1****: AWS locations, measurements, data gaps, sensor type, data periods and environmental settings (T, T_max, T_min = mean, maximum and minimum temperature; RH = relative humidity; PRESS= pressure; SWin, SWin_max = mean and maximum incoming shortwave radiation; SWout = outgoing shortwave radiation; WS and WS_max = mean wind speed and maximum wind speed; WD = wind direction; SnDep = snow depth; SoilTemp and SoilMois = soil temperature and soil moisture; PRECIP = precipitation).*

AWS (elevation m asl)	***Latitude, longitude***	***Variables (% of missing data)***	***Sensors (height; error range)***	***Data period***	***Geomorphic environment***
Ausangate (6349)	*-13.78978*	*T (0.4), T_max (0.4), T_min (3.9), and RH (0.4)*	*Vaisala HMP155 (~2.5 m; ±0.12 °C, ±1.0%)*	*26 July 2022 to 21 November 2022*	*Flat, clean snow surface located in the accumulation zone of the Ausangate Ice Cap*
	-71.23375	*PRESS (0.4)*	*Accubar (~2 m; ±0.3 hPa)*		
		SWin (0.4), SWin_max (0.4)	*Hukseflux NRO1 (2 m; ±2.4 %)*		
		SWout (0.4)	*Hukseflux NRO2 (2 m; ±2.4 %)*		
		WS (0.4), WS_Max (0.4), WD (24)	*RM Young 05108 (2.5 m; ±0.3 m s^{-1})*		
		SnDep (2.5)	*Sommer (2 m; ±0.1 %)*		
Murmurani Alto (5050)	*-13.81105*	*T (0) and RH (7.6)*	*Vaisala HMP45C (1.5 m; ±0.2 °C, ±2 %)*	*4 April 2012 to 9 July 2017*	*Grassland area situated near the inlet of Laguna Sibinacocha*

https://doi.org/10.5194/essd-2026-839
Preprint. Discussion started: 11 November 2026
© Author(s) 2026. CC BY 4.0 License.



	-71.09148	*PRESS (0)*	*Vaisala PTB110 (1.5 m, ±1.0 hPa)*		
		SoilTemp (0)	*CS107 (-10 cm, ±0.4 °C)*		
		SoilMois (0)	*CS616 (-10 cm, ±0.4 °C)*		
		SWin (0.3)	*Apogee SP100 (±5 %)*		
		SnDep (0.7)	*CS SR50A (~1 m, ±1 cm)*		
		Present Weather	*OTT HydroMet Parsivel (1.0 m, ±5 %)*		
Osjollo Anante (5540)	*-13.76714*	*T (0) and RH (0)*	*Vaisala WXT510 (2m, ±0.3 °C, ±3 %)*	*7 April 2012 to 21 July 2015*	*Flat, clean ice surface on the Osjollo Anante Glacier*
	-71.08914	*WS (4) and WD (4)*	*RM Young 05103-45 Alpine (2.5 m, ±3 %)*		
Quelccaya (5650)	*-13.91972*	*T (0) and RH (3.8)*	*EE181(2m, ±0.2 °C)*	*14 October 2014 to 28 September 2025*	*Flat, clean snow surface located in the accumulation zone of the Quelccaya Ice Cap*
	-70.81645	*PRECIP (9.3*)*	*OTT HydroMet Pluvio^2 (2.8 m, ±1 %)*		

https://doi.org/10.5194/essd-2026-839
Preprint. Discussion started: 11 November 2026
© Author(s) 2026. CC BY 4.0 License.



		WS (0), WS_Max (0), and WD (1.1)	*RM Young 05103-45 (3m, ±0.3 m s⁻¹)*		
		SWin (2.5) and SWin_Max (2.5)	*Apogee CS-300 (2m, ±5 %)*		
		SnDep (55.2)	*SR50a (2m, ±1 cm)*		
Lake Sibinacocha (4895)	*-13.92230*	*T (9) and RH (47.4)*	*EE181 (2m, ±0.2 °C)*	*18 July 2017 to 16 August 2026*	*Bare ground situated near the outlet of Laguna Sibinacocha*
	-71.01805	*PRECIP (0.4)*	*OTT HydroMet Pluvio² (1 m, ±0.1 mm)*		
		PRESENT WEATHER	*OTT HydroMet Parsivel (1 m, ±5%)*		
		SWin (3%) and SWin_Max (0)	*Apogee SP100*		
		SnDep (73.0)	*SR50A (2 m, ±1 cm)*		

170

https://doi.org/10.5194/essd-2026-839
Preprint. Discussion started: 11 November 2026
© Author(s) 2026. CC BY 4.0 License.

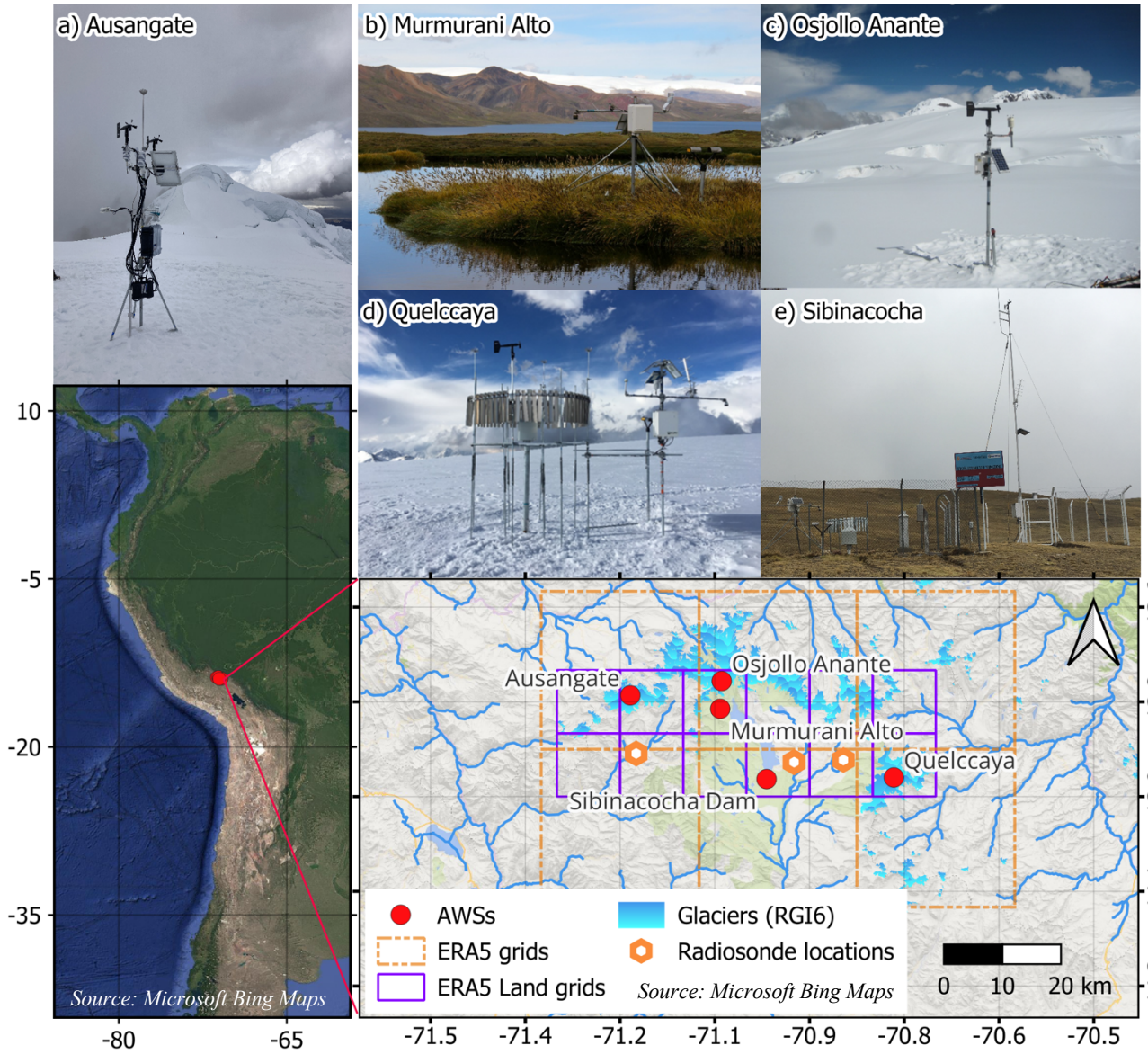


Figure 1: *Locations of automatic weather stations (AWSs), radiosonde releases, ERA5 and ERA5 Land grid boundaries used in analyses presented here, and photos of the AWSs. Background basemap: Microsoft Bing Maps (Virtual Earth), accessed through QGIS, with hill shading. Microsoft product screen shots reprinted with permission from Microsoft Corporation.*

https://doi.org/10.5194/essd-2026-839
Preprint. Discussion started: 11 November 2026
© Author(s) 2026. CC BY 4.0 License.

Open Access Earth System Science Data Discussions

3. Data treatment and uncertainty

The AWS datasets were quality controlled before analysis and publication. Timestamps were checked, invalid and duplicate records were removed, and missing observations were retained as missing values rather than interpolated. Data completeness was calculated separately for each variable and station (Table 1). Seasonal and hydrological-year statistics were only calculated when at least 90% of the expected observations were available. The hydrological year was defined from 1 September to 31 August.

Measurement uncertainty depends on both instrument accuracy and the harsh high-elevation environment. Manufacturer-stated sensor accuracies are provided in Table 1. Air temperature and relative humidity sensors were housed in naturally ventilated radiation shields. These can produce a positive temperature bias during periods of strong solar radiation, high snow albedo, and weak wind (Georges and Kaser, 2002; Matthews et al., 2020), and maximum temperatures under these conditions should therefore be treated cautiously. Snow-depth measurements may also be affected by snow settling, melting, sublimation, wind redistribution, surface roughness, and changes in station height during maintenance.

Precipitation measurements have additional uncertainty because of wind-induced gauge undercatch. The Quelccaya Pluvio² gauge is protected by a Belfort double-alter shield, whereas the Lake Sibinacocha gauge has a single-alter shield. Wind bias corrections were applied following Kochendorfer et al. (2018), and both measured and corrected precipitation are retained in the dataset.

Calculated variables also contain representativeness uncertainty. The 0° isotherm was estimated by linear interpolation between AWS temperatures and therefore assumes a linear temperature gradient between stations. Comparison with seven radiosonde flights indicate that individual estimates may differ somewhat from free atmospheric conditions. Similar representativeness issues apply when comparing point AWS measurements with ERA5 and ERA5-Land grid cells because of differences in elevation, terrain representation, and spatial resolution.

4. Climatological characteristics

The climate of the Cordillera Vilcanota exhibits a pronounced seasonal cycle that can be described using four climatological seasons. September, October, and November (SON) mark the beginning of the hydrological year and the transition into the main wet season; December, January, and February (DJF) represent the core wet season; March, April, and May (MAM) correspond to the transition toward drier conditions; and June, July, August (JJA) represent the main dry season (Perry et al., 2017, 2014).

4.1. Temperature, humidity, and precipitation

The AWS data exhibit this cycle by coherent changes in air temperature, relative humidity, vapour pressure, and precipitation across the elevation gradient (Figs. S1-S3; Tables 2 and S1). At all sites, the warmest and most humid conditions generally occurred during DJF, but daytime temperature maxima often peaked in October and November before the onset of

https://doi.org/10.5194/essd-2026-839
Preprint. Discussion started: 11 November 2026
© Author(s) 2026. CC BY 4.0 License.



the main set season. The coldest and driest atmospheric conditions occurred during JJA; SON and MAM represented the transition into the main wet and drier seasons (Table 2). The daily data also show that dry-season conditions were more variable, particularly for relative humidity and vapour pressure, whereas the rainy season was characterized by persistently high relative humidity (Figs. S1 and S2). The three-year hydrological year means show a strong temperature gradient with elevation.

Precipitation observations at Quelccaya and Lake Sibinacocha further demonstrate the strong seasonality of the regional climate. At Quelccaya, mean seasonal precipitation was 305 mm in SON, 588 mm in DJF, 312 mm in MAM, and only 74 mm in JJA, resulting in a mean hydrological-year total of 1279 mm. Thus, 46% of the annual precipitation occurred during DJF alone, whereas only about 6% occurred during JJA. At Lake Sibinacocha, mean precipitation totals were 161 mm in SON, 383 mm in DJF, and 177 mm in MAM, and 22 mm in JJA. The mean hydrological year precipitation total at Lake Sibinacocha was 743 mm. Correcting the Quelccaya precipitation measurements for gauge undercatch using the transfer function from Kochendorfer et al. (2018) increased the mean hydrological-year precipitation from 1279 to 1412 mm (+10.4%), but did not alter the overall seasonal pattern, with DJF remaining the wettest and JJA the driest season. The Kochendorfer et al. (2018) undercatch correction for the single alter shield around the Lake Sibinacocha gauge increased the precipitation total from 764 to 936 mm (+23%) during the 2018 hydrological year.

Table 2*: Seasonal (SON = September, October, and November; DJF = December, January, and February; MAM = March, April, and May; JJA = June, July, and August) and annual (September to August -- hydrological year) mean temperature (T) at four automatic weather stations (AWSs) and precipitation (PRECIP) for two AWSs. Statistics are presented for September 2012–August 2015 at Murmurani Alto and Osjollo Anante, and for September 2018–August 2021 at Quelccaya and Lake Sibinacocha. Seasonal or annual mean values are discarded when data gaps exceed 10% of the data period. *JJA retained despite 85% coverage; 12-day gap in June 2018.*

Variables	Stations	SON	DJF	MAM	JJA	Annual mean/total
T (°C)	Murmurani Alto (5,050 m)	1.5	1.9	1.7	-0.3	1.2
T (°C)	Osjollo Anante (5,540 m)	-2.5	-2.1	-2.5	-	-2.7
T (°C)	Quelccaya (5,650 m)	-3.9	-2.9	-3.7	-5.6	-4.0
T (°C)	Lake Sibinacocha	2.3	2.9	2.7	0.8	2.2

https://doi.org/10.5194/essd-2026-839
Preprint. Discussion started: 11 November 2026
© Author(s) 2026. CC BY 4.0 License.



	(4,895 m)					
PRECIP (mm)	Quelccaya (5,650 m)	305	588	312	74	1279
PRECIP (mm)	Lake Sibinacocha (4,895 m)	161	383	177	22*	743

230

4.2 Wind speed and direction from Osjollo Anante and Quelccaya

W and NW flow predominated at Osjollo Anante, especially during austral fall (MAM) and winter (JJA), when wind speeds were also the highest (Fig. 2). NW and NNW flow represented ~20% of all hours in the core of the wet season in austral summer (DJF) but remained mainly light at less than 4 m s^{-1}. Except for predominant NW flow in the austral winter (JJA), the
235 prevailing flow was E and SE at Quelccaya the remainder of the year and especially in the wet season (DJF) (Fig. 3). These results are largely consistent with channeled upslope flow through major interandean valleys as a connector between the Amazon and Andes (Junquas et al., 2018, Chavez and Takahashi 2017, Perry et al., 2017, 2014). The river systems and associated valleys drop to the NW to the Amazon from Osjollo Anante and to the E and SE from Quelccaya (Fig. 1). The dominant NW flow in the austral winter (JJA) likely results from strong synoptic-scale flow and reduced moisture transport
240 from the Amazon basin (e.g., Garreaud et al. 2003).

https://doi.org/10.5194/essd-2026-839
Preprint. Discussion started: 11 November 2026
© Author(s) 2026. CC BY 4.0 License.

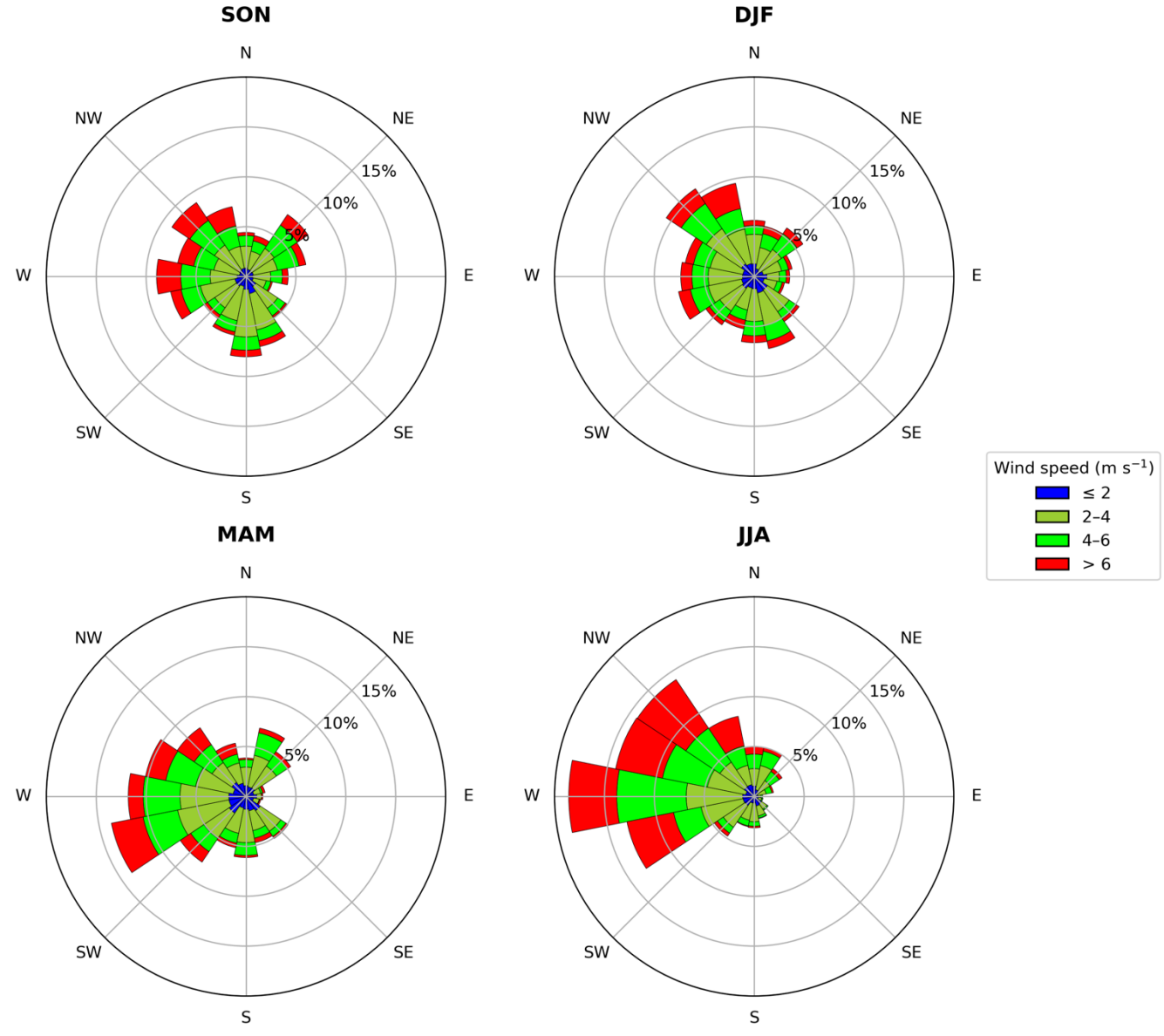


Figure 2: Seasonal wind-rose for Osjollo Anante based on hourly wind speed (m s^{-1}) and direction (degrees) observations from September 2012 to August 2015. Seasons are grouped as September, October, November (SON), December, January, February (DJF), March, April, May (MAM), and June, July, August (JJA). Radial axes show the percentage frequency of valid hourly observations within each season.

https://doi.org/10.5194/essd-2026-839
Preprint. Discussion started: 11 November 2026
© Author(s) 2026. CC BY 4.0 License.

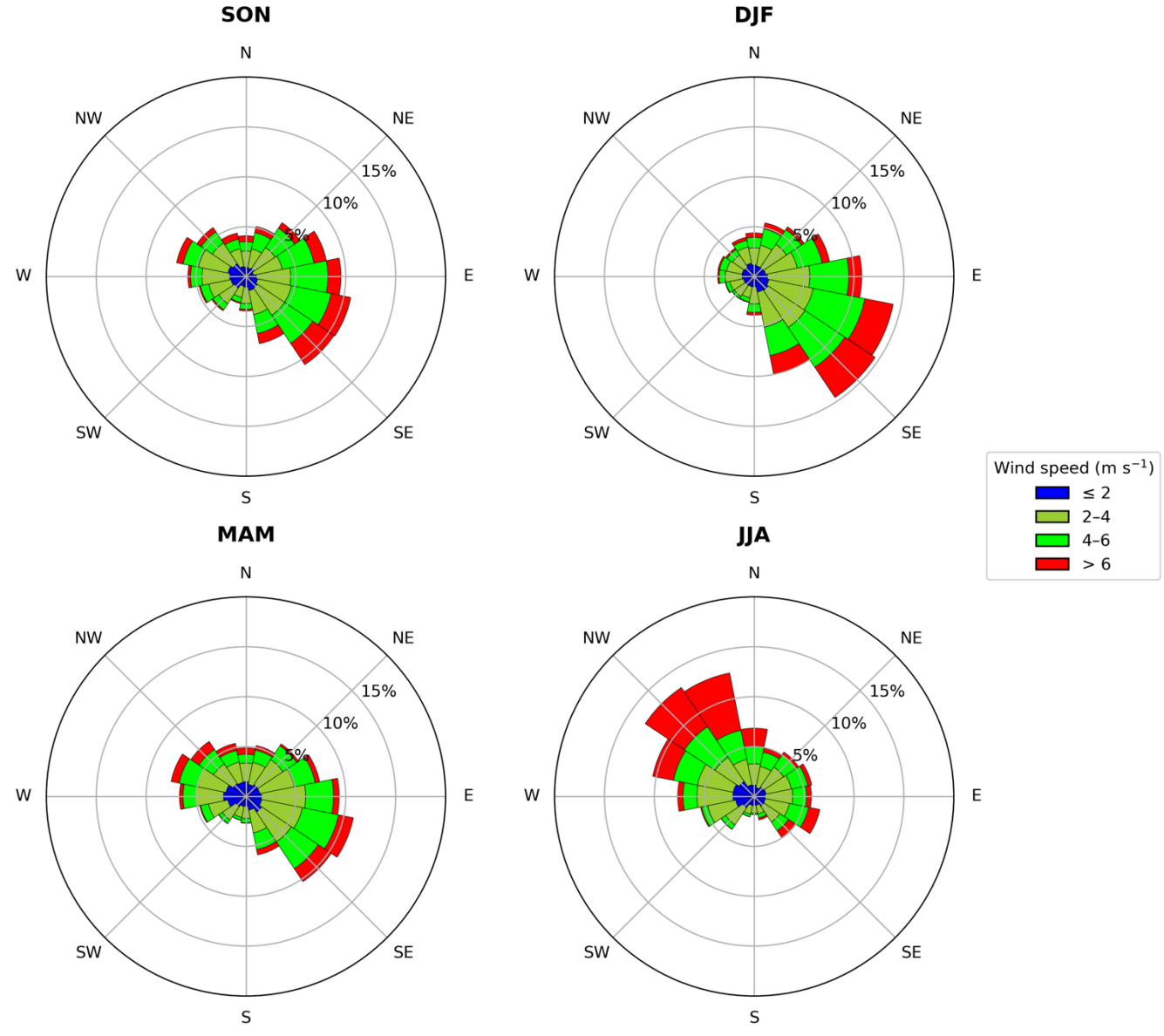


Figure 3: Seasonal wind rose for Quelccaya based on hourly wind speed (m s^{-1}) and direction (degree) observations from September 2014 to August 2025. Seasons are grouped as September, October, November (SON), December, January, February (DJF), March, April, May (MAM), and June, July, August (JJA). Radial axes show the percentage frequency of valid hourly observations within each season.

https://doi.org/10.5194/essd-2026-839
Preprint. Discussion started: 11 November 2026
© Author(s) 2026. CC BY 4.0 License.



4.3 Vertical gradients in temperature, precipitation, and vapor pressure

The Murmurani Alto and Osjollo Anante AWSs, separated by approximately 5 km with an elevation difference of 490 m, provide an opportunity to evaluate vertical gradients and elevation dependency in temperature and moisture. Both locations exhibited closely synchronized daily and seasonal variability between April 2012 and March 2015 (Fig. S1). Temperature increases and decreases occurred at nearly the same time at both stations, indicating that they were influenced by the same regional atmospheric conditions. As expected, Osjollo Anante remained consistently colder than Murmurani Alto throughout the observation period, with mean temperatures of −2.5, −2.1, and -2.5°C in SON, DJF, and MAM, respectively, compared with 1.5, 1.9, and 1.7°C at Murmurani Alto. The average temperature difference between the stations was therefore 3.9°C, a near-surface lapse rate of -8.0°C km^{-1}. Lower temperatures at Murmurani Alto were very infrequent, accounting for only 2% of all hourly observations, and occurred mostly between 0100-1100 UTC (8:00 pm to 6:00 am LST). Mean seasonal near-surface lapse rates ranged from -7.3°C km^{-1} in JJA to -8.5°C km^{-1} in MAM, while the 0°C isotherm varied from 4,975 m in JJA to 5,277 m in DJF (Table S2).

Characterization of vertical gradients of temperature are also possible for Quelccaya and Lake Sibinacocha, with a separation of approximately 22 km and 755 m in elevation. A similarly coherent seasonal cycle with substantial differences in absolute meteorological conditions were evident (Fig. S2). Daily mean temperatures at Quelccaya remained below freezing throughout the year, with seasonal temperatures ranging from −5.6°C in JJA to −2.9°C in DJF, whereas Lake Sibinacocha ranged from 0.8 to 2.9°C. Their hydrological year mean temperatures were −4.0°C and 2.2°C, respectively. Lower temperatures at Phinaya were very infrequent, amounting to only 0.7% of all hourly observations and occurring mostly between 0300-1100 UTC (10:00 pm to 6:00 am LST). Mean seasonal near-surface lapse rates observed between Quelccaya and Lake Sibinacocha were similar to those for Murmurani Alto and Osjollo Anante. Temperature gradients ranged from -7.6°C km^{-1} in DJF to -8.5°C km^{-1} in JJA, and the 0°C isotherm ranged from 4,993 to 5,270 m.

The vertical gradient in precipitation between Lake Sibinacocha and Quelccaya was positive, at +710 mm km^{-1}, likely reflecting downslope shadowing at Lake Sibinacocha. At Quelccaya, mean precipitation was 305 mm in SON, increased to 588 mm in DJF, declined to 312 mm in MAM, and was only 74 mm in JJA (Fig. S3). The mean hydrological year precipitation total was 1279 mm. DJF therefore accounted for approximately 46% of the annual precipitation, while JJA contributed only about 6%. At Lake Sibinacocha, mean seasonal precipitation was 161 mm in SON, 383 mm in DJF, and 177 mm in MAM. A representative JJA mean was 22 mm with 85% data coverage (12-day data gap in June 2018), although the mean hydrological year precipitation total was 743 mm.

Vapor-pressure gradients were negative throughout the year at both transects and were strongest during DJF, reaching -2.0 hPa km^{-1} at Murmurani–Osjollo and -1.9 hPa km^{-1} at Quelccaya–Sibinacocha, while the weakest gradients occurred during JJA (-0.7 and -0.9 hPa km^{-1}, respectively). The 6.11 hPa isoline was most consistently resolved during DJF and MAM, occurring at 4,326 to 4,687 m for Murmurani Alto to Osjollo Anante and 4,540 to 4,805 m for Lake Sibinacocha to Quelccaya. Together, the two transects show a coherent seasonal structure in freezing-level and atmospheric-moisture gradients across the Cordillera Vilcanota, while also highlighting the influence of local topography and exposure on near-surface meteorological

https://doi.org/10.5194/essd-2026-839
Preprint. Discussion started: 11 November 2026
© Author(s) 2026. CC BY 4.0 License.


conditions. Temperature and vapor pressure gradients were calculated based on the average daily temperature and relative humidity at (a) Murmurani and Osjollo (Figs. S4 and S5) and b) Quelccaya and Sibinacocha (Figs. S6 and S7). Quantification of these gradients highlights the value of installing and maintaining AWSs at different elevations in close horizontal distances.

4.4 0°C isotherm elevation and upper air soundings

The 0°C isotherm elevation derived from the temperature gradient between Quelccaya and Lake Sibinacocha was compared with seven radiosonde observations collected between 4 and 7 March 2018 (Figs. S8; Table S4). The radiosonde-derived 0°C isotherm elevations ranged from 4,959 to 5,440 m, whereas the linearly interpolated estimates from the AWS stations ranged from 5,071 to 5,597 m. Overall, the two methods showed reasonable agreement, with a mean bias (radiosonde minus AWS) of approximately −8 m, a mean absolute error (MAE) of 116 m, and RMSE of 134 m. The differences between the two estimates also varied with the time of observation (Table S4). Radiosonde measurements were obtained between 00:00 and 19:00 UTC, corresponding approximately to 19:00 of the previous day to 14:00 local time (UTC−5). The two daytime observations at 18:00 and 19:00 UTC (approximately 13:00–14:00 LST) produced AWS-derived isotherm elevations that were 157 and 165 m higher, respectively, than the radiosonde estimates. In contrast, several evening observations around 0000 UTC (approximately 19:00 local time) showed lower AWS-derived isotherm elevations than the radiosonde, with differences of approximately 29, 121, and 213 m. The smallest difference was observed at 01:00 UTC on 5 March, when the radiosonde and AWS estimates differed by only 15 m.

This time-of-day dependence likely reflects differences in the diurnal response represented by the two approaches, which is well documented in mountain regions (Barry et al., 2008). The AWS-derived isotherm is calculated from near-surface temperatures at two mountain elevations and can therefore respond strongly to daytime surface heating and nighttime cooling, whereas the radiosonde-derived isotherm represents the vertical free atmospheric temperature profile at the time of the sounding. Consequently, differences in boundary layer development and surface heating may contribute to larger discrepancies during some periods of the day. However, given the small number of coincident observations, the apparent diurnal pattern should be interpreted cautiously. Overall, the comparison indicates that the two AWS method provides a reasonable representation of local 0°C isotherm elevation, while individual estimates can differ by more than 100–200 m depending partly on short-term atmospheric and diurnal conditions.

4.5 Quelccaya and Lake Sibinacocha hydrological year summaries

Snow accumulation at Quelccaya showed substantial interannual variability over the six hydrological years examined (Fig. 4; Table 3). For the five hydrological years with complete precipitation records, the annual precipitation varied from 1020 mm in 2015-2016 to 1,377 mm in 2018-2019, whereas the mean annual temperature varied from -2.9°C (2015-2016) to

https://doi.org/10.5194/essd-2026-839
Preprint. Discussion started: 11 November 2026
© Author(s) 2026. CC BY 4.0 License.



-4.6°C (2020-2021). Due to COVID-19 pandemic travel restrictions, the Quelccaya Pluvio^2 weighing precipitation gauge could not be emptied in 2020 and reached its capacity before the end of the wet season.

The variation in snow depth shows that the hydrological years generally began with net snow ablation before the start of the core of the wet season (DJF), consistent with the findings of Hurley et al. (2019). The minimum occurred later in 2015–2016 (−0.49 m; 30 November), whereas in other hydrological years the minimum snow depth occurred in between September and early October in 2016–2017 (−0.22 m; 22 September), 2017–2018 (−0.14 m; 11 September), 2018–2019 (−0.15 m; 24 September), and 2019–2020 (−0.33 m; 1 October). Following these initial losses, snow depth generally increased with cumulative precipitation, although the magnitude and timing of accumulation differed markedly among years (Fig. 4).

End-of-year net snow accumulation was not directly proportional to total annual precipitation. The largest net accumulation occurred in 2017–2018 (2.19 m), when total precipitation was 1,247 mm and mean temperature was −4.4°C. Similarly, 2016–2017 accumulated 1.95 m from 1,234 mm of precipitation. In contrast, 2018–2019 received the highest precipitation total (1,377 mm) but ended with only 1.32 m of net snow accumulation, while 2019–2020 recorded 1,213 mm of precipitation and 1.39 m of accumulation. The clearest contrast occurred in 2015–2016, the warmest year (−2.9°C), which ended with a slightly negative net snow-depth change (−0.09 m) despite receiving 1,020 mm of precipitation.

These differences suggest that net annual snow accumulation at Quelccaya reflects not only the amount of precipitation received but also the thermal conditions of precipitation and snow ablation during the hydrological year. Years with relatively cold conditions, particularly 2016–2017 and 2017–2018, accumulated substantially more snow, whereas the comparatively warm 2015–2016 hydrological year experienced little net accumulation. In fact, our temperature and snow depth data indicate that substantial rain and rain/snow mix fell at the Quelccaya AWS in February 2016 (Fig. S9). The combined evolution of air temperature, cumulative precipitation, and snow depth therefore highlight the importance of both snow accumulation and temperature-index modeling at the site.

https://doi.org/10.5194/essd-2026-839
Preprint. Discussion started: 11 November 2026
© Author(s) 2026. CC BY 4.0 License.

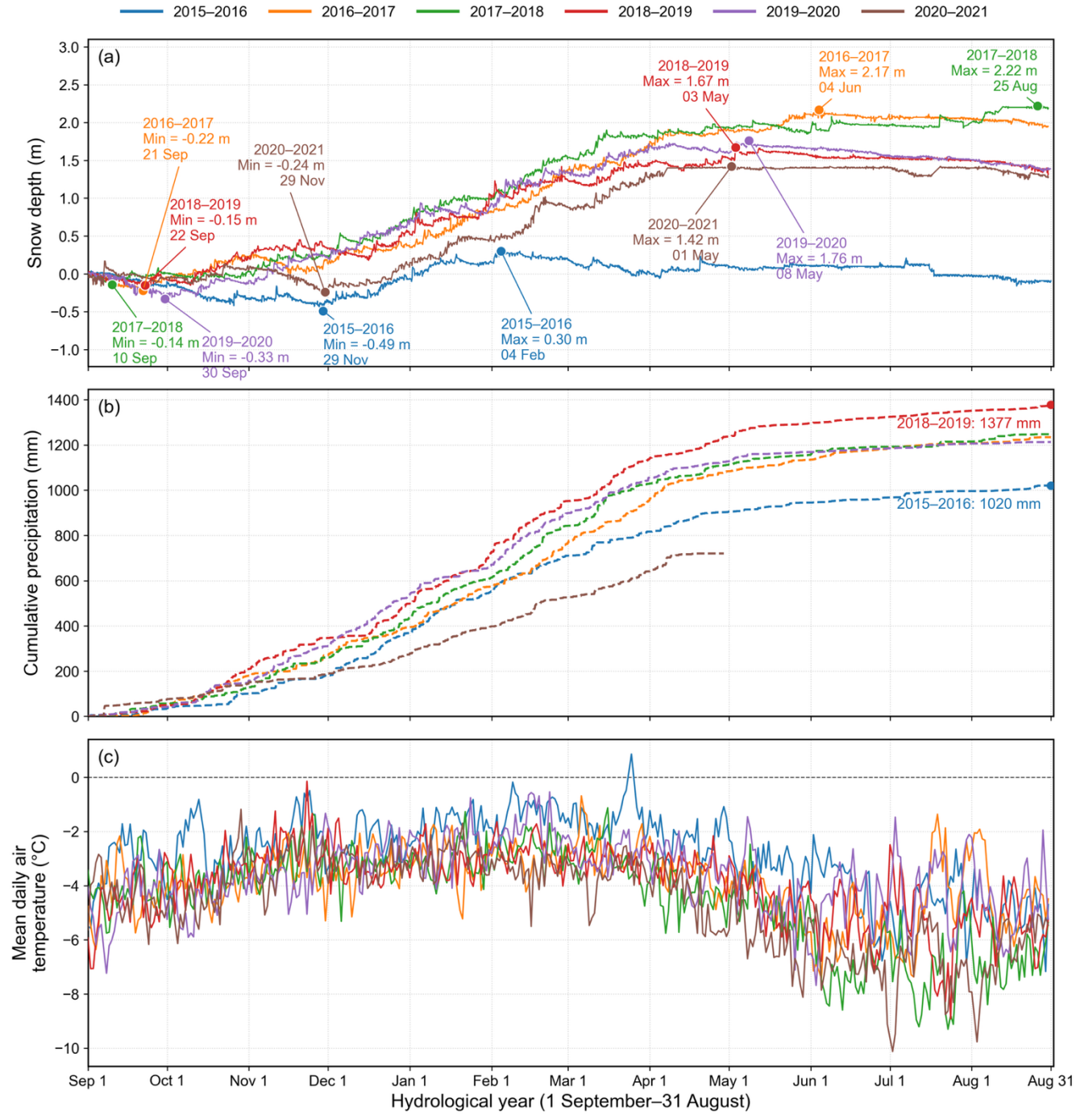


Figure 4: *Snow depth (a), the cumulative precipitation (b), and mean daily air temperature (c) from the Quelccaya AWS for different hydrological years.*

345

https://doi.org/10.5194/essd-2026-839
Preprint. Discussion started: 11 November 2026
© Author(s) 2026. CC BY 4.0 License.



Open Access Earth System Science Data Discussions

***Table 3**: Precipitation, annual temperature and snow accumulation/ablation for each hydrological year between 2015 and 2021 from the Quelccaya AWS.*

	Quelccaya			
Hydrological year	Total Precipitation (mm)	Mean Temperature (°C)	Net accumulation (m) at the end of hydrological year	Minimum snow depth (m) and respective date
2015-2016	1020	-2.9	-0.09	-0.49 11/30/2015
2016-2017	1234	-3.9	1.95	-0.22 9/22/2016
2017-2018	1247	-4.4	2.19	-0.14 9/11/2017
2018-2019	1377	-3.9	1.32	-0.15 9/24/2018
2019-2020	1213	-3.7	1.39	-0.33 10/1/2019
2020-2021*	720	-4.6	1.4/1.28	-0.18 11/30/2020
	720 mm is only until the end of April		1.40 m (30 April)/1.28 m (31 August)	

Hydrological year precipitation totals at Lake Sibinacocha ranged from 582 mm in 2022-2023 to 967 mm in 2021-22 (Fig. S10). Monthly and annual totals generally compared favorably to the co-located SENAMHI tipping bucket gauge (Fig. S11). Differences in the daily timing of precipitation were noted due to the delay in melting and thereby recording solid precipitation until the next morning in the unheated tipping bucket (Fig. S12). The observed Quelccaya-Sibinacocha precipitation ratio exhibited considerable variability, ranging from 1.5 to 2.0 from 2018 to 2020, remaining close to 1 from 2021 to 2023, and returning to ~1.5 in 2025 (Fig. 5). Covid-era travel and budget restrictions prevented proper maintenance and emptying of the Pluvio^2 bucket in 2020, leading to loss of precipitation data in 2021 after the bucket reached its capacity. Firn densification and flow in 2021 and 2022 caused the vertical pipes that serve as the base of the Pluvio^2 and Belfort double alter shields to tilt away from vertical, introducing some likely measurement errors. We therefore encourage users to review the metadata carefully when deciding which time periods to use and what corrections may be required. The Quelccaya-Sibinacocha precipitation ratio suggests that the annual maintenance and raising of the AWS in 2023 may have restored the precipitation measurements to pre-Covid-19 quality, with ratios of ~1.5 in 2024-2025.

https://doi.org/10.5194/essd-2026-839
Preprint. Discussion started: 11 November 2026
© Author(s) 2026. CC BY 4.0 License.

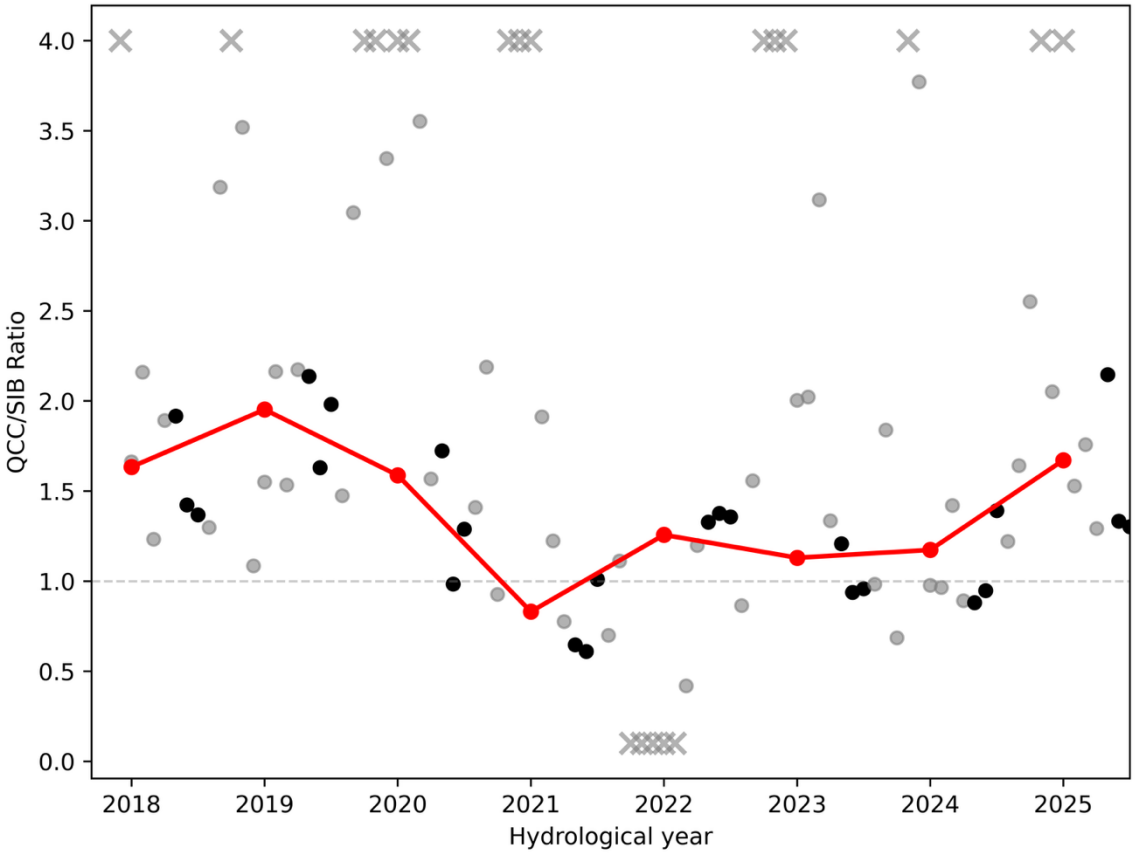


Figure 5: Ratio of measured precipitation (uncorrected) between Quelccaya and Sibinacocha for each month; black dots represent summer months (DJF, most precipitation) and gray dots the remaining months. X markers are months where the ratio is greater than 4 or less than 0.1. The red line represents the ratio of Quelccaya/Sibinacocha precipitation for each hydrological year and each marker is centered in September of each year.

4.6 Murmurani Alto precipitation and snowfall observations

The meteorological observations and snowfall characteristics described in this section were previously summarized in Poremba et al. (2015). Co-location of the Murmurani Alto AWS with manual precipitation and snowfall observations from a citizen science observer (Guy et al., 2019) allowed for a direct comparison and analysis of precipitation event characteristics. In the two years between 1 July 2012 and 30 June 2014, snowfall at Murmurani Alto averaged 467 cm (431 cm in 2012-2013 and 502 cm in 2013-2014) as recorded by an acoustic snow depth sensor, and LE precipitation averaged 686 mm (623 mm in

https://doi.org/10.5194/essd-2026-839
Preprint. Discussion started: 11 November 2026
© Author(s) 2026. CC BY 4.0 License.



2012-2013 and 749 mm in 2013-2014), recorded by the observer (Table 4). Most of the precipitation occurred during the peak months of the austral wet season (DJF, Fig. S13). Snowfall exceeded 80 cm in several months during the wet seasons, with nearly 120 cm accumulating in January 2014. New snowfall density averaged 147 kg m^{-3}, with very little variation between the two years. Snowfall events were typically light (2.6 cm per event over the period of study), but frequent, with precipitation a near-daily occurrence during the wet season. Even though precipitation was nearly exclusively solid at Murmurani Alto, snowfall was highly ephemeral and typically ablated quickly during daylight hours with the high solar elevation of the tropical sun, relatively low albedo, and presence of abundant water in the *bofedale*. The maximum snow depth recorded during the period was 17 cm. Snow was the primary precipitation type, but graupel also constituted a significant number of precipitation hours. In some months, graupel accounted for over half of the precipitating hours, particularly during the dry season (Fig. S13). Although liquid precipitation (rain) was infrequent (5% of precipitation hours; Table 4), its presence is noteworthy at 5,050 m, as many glacier termini in the Cordillera Vilcanota extend to lower elevations, commonly around 4,700 to 5,000 m (Davies et al., 2026). Although rainfall contributes relatively little direct energy to glacier melt, it does not replenish highly reflective snow cover, leaving lower albedo ice exposed to absorb more solar radiation and accelerate melting (Favier et al., 2004).

Table 4: Summary of snowfall and precipitation at Murmurani for 2012-13, 2013-14, and the entire period of record. These totals do not include April to June 2012. Separate snowfall events required a 3-hr minimum break in precipitation as identified by the Parsivel disdrometer. Reproduced from Poremba et al. (2015).

Variables	**2012-2013**	**2013-2014**	**Mean**
Snowfall (cm)	431	502	467
Precipitation (mm)	623	749	686
New snowfall density (kg m^{-3})	145	149	147
Number of snowfall events	159	197	178
Mean snowfall per event (cm)	2.7	2.5	2.6
Maximum snow depth (cm)	17	17	17

4.7 Precipitation phase at Lake Sibinacocha

A longer record of precipitation phase and intensity from 2017 to 2026 is available from the Lake Sibinacocha AWS. Individual hydrological year and mean monthly frequency of precipitation classes (Fig. 6) show a very similar pattern to Murmurani Alto, except for slightly higher percentages of rain due to its 155 m lower elevation and proximity to Lake Sibinacocha. Rain frequency ranged from 12.8% in 2019 to 35.8% in 2024. The months of February and March showed the highest frequency of rain (~23%), with rain nearly completely absent during the austral winter months of June, July, and

https://doi.org/10.5194/essd-2026-839
Preprint. Discussion started: 11 November 2026
© Author(s) 2026. CC BY 4.0 License.



Open Access Earth System Science Data Discussions

August. As at Murmurani Alto, graupel was the most observed precipitation type, accounting for 33% of all precipitation hours and very little interannual or seasonal variability. May, July, and August exhibited the lowest frequency of graupel, averaging ~25%. The very high frequency of graupel in our longer-term observations confirms its climatological significance previously reported by Perry et al. (2017) using a shorter period of observations and highlights the presence of abundant supercooled liquid water in the feeder clouds during afternoon convection and nighttime stratiform precipitation events. In other mountain environments, graupel is associated with more intense precipitation associated with convective instability, lightning, and heavy riming (e.g., Pujol et al., 2005), thereby requiring care in the interpretation of water isotopes (δ^{18}O, HD) in the Cordillera Vilcanota and broader tropical Andes.

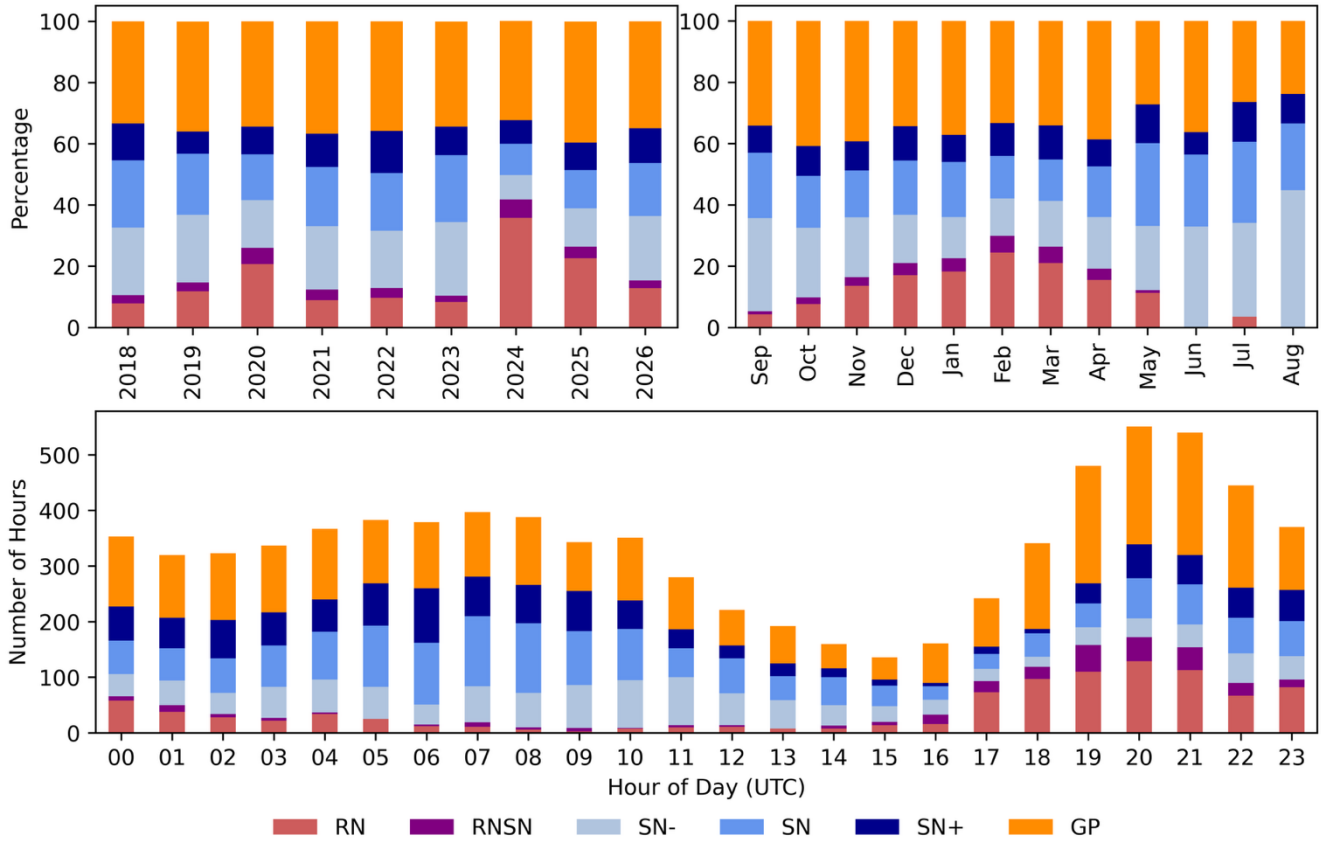


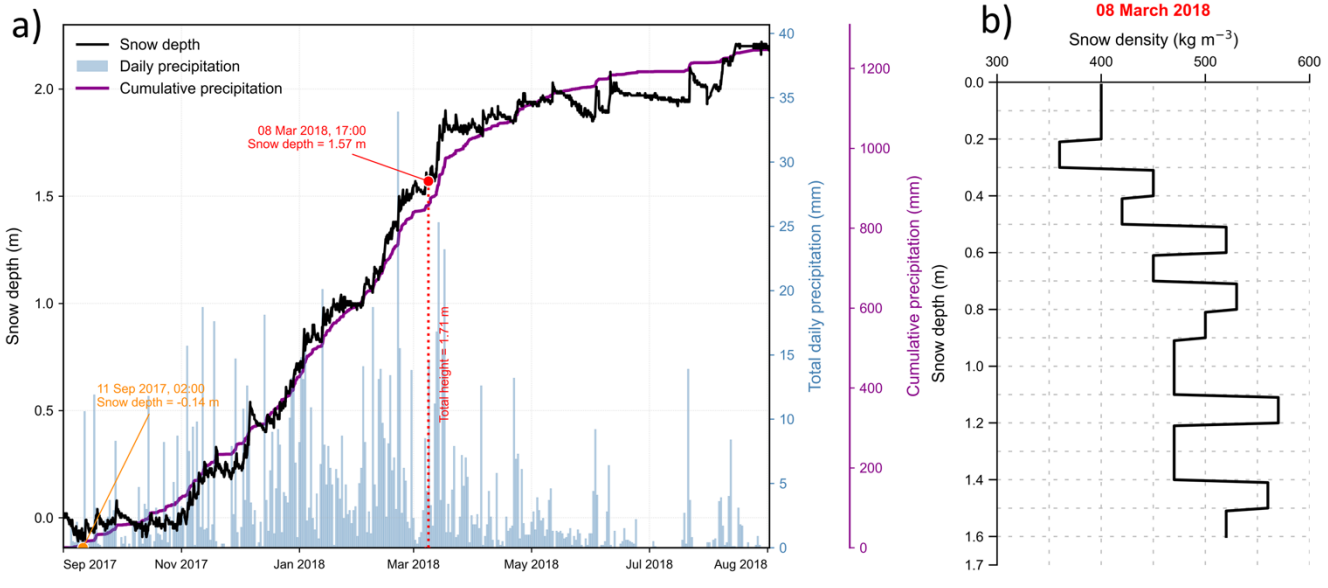
Figure 6: Parsivel precipitation codes at Lake Sibinacocha for (a) percentage of precipitation type for all hours during 2018 to 2026 hydrological years, (b) percentage of precipitation type for all hours during each month between August 2017 and July 2026, and (c) daily composite by time of day for the number of hours according to precipitation type. GP graupel; SN+ heavy snow; SN moderate snow; SN- light snow; RN/SN rain/snow mix; RN rain.

https://doi.org/10.5194/essd-2026-839
Preprint. Discussion started: 11 November 2026
© Author(s) 2026. CC BY 4.0 License.

5. 2017-18 Snow Pit Observations vs. Observed Precipitation

Snow accumulation at the Quelccaya AWS site was assessed using precipitation, snow-depth, and snow pit density measurements for 1 September 2017 to 31 August 2018, with particular emphasis on conditions through the 8 March 2018 snow pit measurement (Fig. 7). Referenced to 0 m on 1 September, snow depth initially declined to −0.14 m on 11 September, reflecting surface lowering due to ablation, settling, and/or wind erosion, before increasing to 1.57 m by 8 March. Thus, surface height increased by 1.71 m between 11 September and 8 March. Cumulative precipitation totaled approximately 857 mm LE by 8 March, including ~7 mm LE from 1-11 September and ~851 mm LE from 11 September 2017 to 8 March 2018; annual precipitation through 31 August 2018 was 1,247 mm LE. The 8 March 2018 snow pit sampled approximately 1.6 m of snowpack, with densities ranging from 360 to 570 kg m^{-3} and a profile-average density of 472.5 kg m^{-3}.

Applying the mean snow pit density to the 1.71 m increase in surface height yields an estimated accumulation of approximately 808 mm SWE between 11 September 2017 and 8 March 2018, 43 mm less than the 851 mm LE of measured precipitation over the same period. This apparent mass-balance residual may reflect sublimation, wind-driven snow redistribution, snow settling, precipitation undercatch, and/or spatial differences between the AWS and snow pit locations. Nonetheless, the very close agreement in LE precipitation and snowpack SWE provides high confidence in the Pluvio^2 LE precipitation totals. The 0.14 m surface lowering from 1–11 September 2017 corresponds to ~66 mm SWE using the mean snow pit density, despite ~7 mm LE of precipitation during this period. The net surface loss therefore indicates that ablation, wind erosion, and/or settling exceeded precipitation inputs during the first 10 days of the analysis period.



https://doi.org/10.5194/essd-2026-839
Preprint. Discussion started: 11 November 2026
© Author(s) 2026. CC BY 4.0 License.



Figure 7: a) Snow depth versus cumulative precipitation, along with daily precipitation, at the Quelccaya AWS between 1 September 2017 and 31 August 2018. The two vertical dotted lines represent the minimum snow height on 11 September 2017 and the snow depth during the snow pit sampling on 8 March 2018. b) Snow density as a function of depth.

6. Comparison with ERA5 and ERA5 Land precipitation

Annual totals from the AWSs, including both uncorrected and corrected precipitation totals, were compared with the nearest pixel centroid in ERA5 and ERA5 Land over the data available period at the measurements (Fig. 8). This variability demonstrates that precipitation is strongly influenced by local elevation and spatial differences that are difficult to resolve within reanalysis grid cells. The cumulative hydrological year precipitation curves show differences not only in annual totals but also in the seasonal timing of accumulation (Fig. 9). At both stations, AWS precipitation generally showed a marked reduction after May, whereas the reanalysis products maintained precipitation during the latter part of the hydrological year. Differences between ERA5 and ERA5 Land were particularly evident at the higher Quelccaya AWS, indicating that the two products do not represent high-elevation precipitation in the same way, likely due to differences in grid resolution and elevation. Higher wind speeds at the more open and exposed Quelccaya site may also introduce greater uncertainty in the precipitation measurements, even after correcting for undercatch. The AWS observations therefore remain essential for evaluating and constraining reanalysis products in the tropical high Andes, as demonstrated for ERA5 and other reanalysis models in Birkel et al. (2022).

https://doi.org/10.5194/essd-2026-839
Preprint. Discussion started: 11 November 2026
© Author(s) 2026. CC BY 4.0 License.

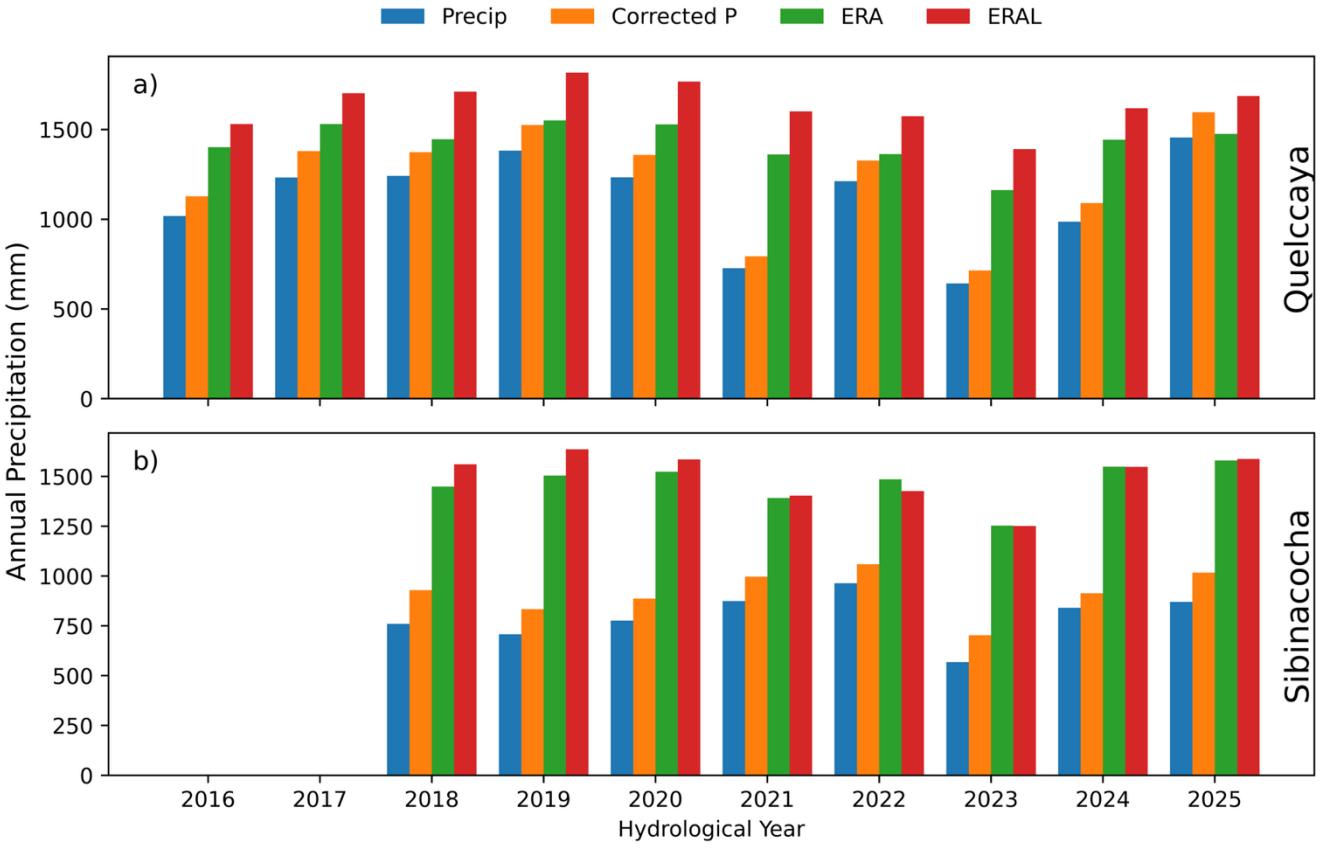


Figure 8: Annual total precipitation in (a) Quelccaya and (b) Sibinacocha comparing observations from the AWS (uncorrected in blue and corrected in orange) to reanalysis products, ERA5 (green) and ERA5-Land (red).

https://doi.org/10.5194/essd-2026-839
Preprint. Discussion started: 11 November 2026
© Author(s) 2026. CC BY 4.0 License.

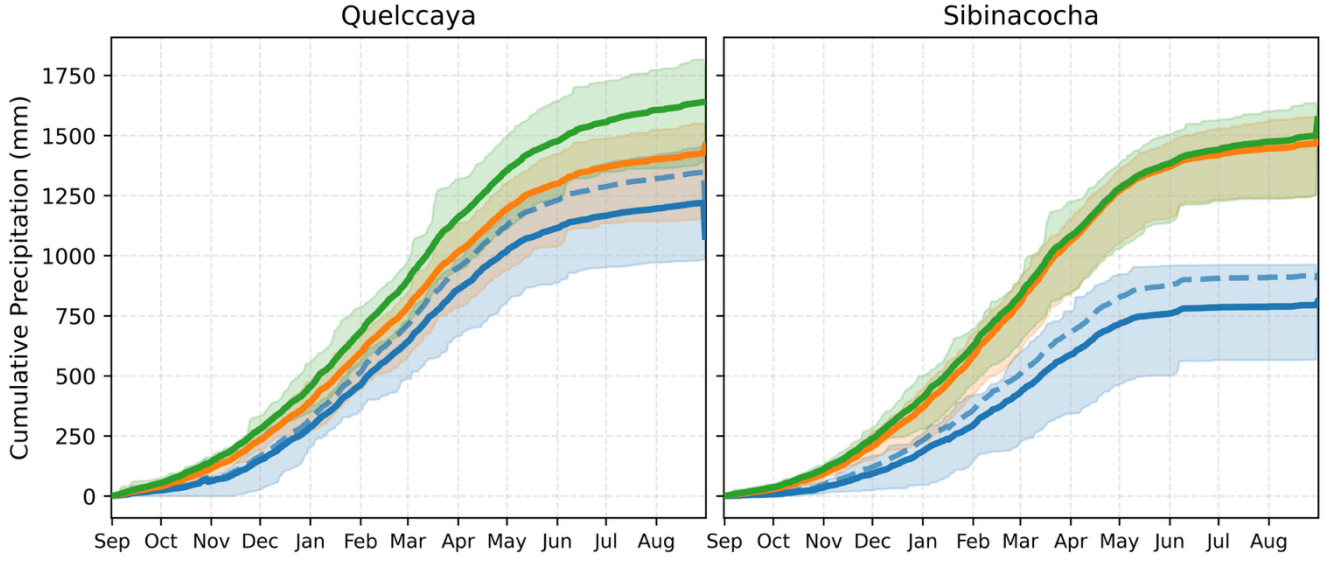


Figure 9: Annual cumulative precipitation comparison between the Quelccaya (left) and Lake Sibinacocha (right) and ERA5/ERA 5-Land. The mean over all the years is solid and the minimum and maximum of all the hydrological years is shaded. Quelccaya data are from 2016-2020, 2022 and 2024-2025 and Lake Sibinacocha from 2017-2025. ERA5/ERA5-Land products were used for the same periods.

7. Conclusions

Meteorological records from the Cordillera Vilcanota AWS network provide rare in situ observations of temperature, humidity, precipitation, snow depth, and wind at very high elevations, revealing strong seasonal and short-term variability in the tropical Andean atmosphere and cryosphere. A pronounced dry season (June to August) contrasts with a warmer, more humid wet season (December to February), when most of the annual precipitation occurs. The 0°C isotherm linearly interpolated from the Quelccaya–Sibinacocha temperature varied substantially over short timescales and agreed closely with seven nearby radiosonde profiles collected from 4 to 7 March 2018 (mean bias −8 m). Net snow accumulation closely corresponded to precipitation at Quelccaya during 2017-2018, but interannual records show that snow accumulation does not scale directly with precipitation totals in all years, particularly for the very strong warm-phase ENSO (El Niño) year of 2015-16. Collectively, these findings underscore the importance of sustained high-elevation observations for resolving the rapidly varying processes controlling precipitation phase and snow accumulation in tropical glacier environments.

https://doi.org/10.5194/essd-2026-839
Preprint. Discussion started: 11 November 2026
© Author(s) 2026. CC BY 4.0 License.



Data Availability

The quality-controlled AWS datasets are freely available at https://doi.org/10.5281/zenodo.23315967 (Perry et al., 2026). The raw disdrometer, sounding data, and the snow pit data are also available. The code that was used to prepare the datasets and compute statistics is available at https://doi.org/10.5281/zenodo.23813420

Author Contributions

LBP, AS, and TM conceptualized the project, curated data, acquired funding, and led fieldwork. SA, HG, MR, NM, and CC assisted with the installations, maintenance, and data download from the AWSs and snow pit sampling. HG led radiosonde releases. AK and LCF led data analysis and code development. LBP, AK, and LCF prepared the manuscript with contributions from all co-authors. WS managed maintenance and data download for the Quelccaya AWS.

Competing Interests

The authors declare that they have no conflicts of interest.

Acknowledgements

This work was supported by U.S. National Science Foundation grants AGS 1347179 and AGS 1566450, the Justin Brooks Fisher Foundation, and the National Geographic Society. Appalachian State University summer study abroad students (2012-2014) assisted with maintenance and data download of the Murmurani Alto and Osjollo Anante stations. The authors are grateful to citizen science observer P. Godofredo for taking daily precipitation measurements and for permission to install an AWS on his land in Murmurani Alto. The authors acknowledge the helpful guidance and field support from Adrían Ccahuana, Alfredo Ccahuana, Raul Ccahuana, Pedro Choque, Paulino Choque, Christian Crispin, David Crispin Condori, Felipe Crispin Condori, Gumercindo Crispin Condori, Eric Burton, Jason Endries, Barry Goodison, Ben Graves, Doug Hardy, Cecilia Llusco, Senobia Llusco, Daniel Martin, Paul Mayewski, Evan Montpellier, Alex Moore, Ruthmery Pillco, Laura Ticona, and Alfredo Tupayachi. The late Lonnie Thompson was instrumental in inspiring the fieldwork and installation of the AWSs. During the High-Elevation Climate Science Workshop in Incline Village, NV, in June 2026, he also strongly encouraged the lead author to synthesize and publish these datasets. We acknowledge his remarkable life and extraordinary contributions to science and society.

References

Andrade, M. and Laj, P.: Life in a Global Atmospheric Watch Station: Watching the Air from the Top of the Andes, WMO Bulletin, 75, https://wmo.int/resources/wmo-bulletin/wmo-bulletin-vol-7501-air-issue/life-global-atmospheric-watch-station-watching-air-from-top-of-andes (last access: 10 October 2026), 2026.

Barry, R. G.: Mountain weather and climate, 3rd edn., Cambridge University Press, Cambridge, UK,

© Author(s) 2026. CC BY 4.0 License.



https://doi.org/10.1017/CBO9780511754753, 2008.

Birkel, S. D., Mayewski, P. A., Perry, L. B., Seimon, A., and Andrade-Flores, M.: Evaluation of reanalysis temperature and precipitation for the Andean Altiplano and adjacent Cordilleras, Earth Space Sci., 9, e2021EA001934, https://doi.org/10.1029/2021EA001934, 2022.

Chavez, S. P. and Takahashi, K.: Orographic rainfall hot spots in the Andes-Amazon transition according to the TRMM precipitation radar and in situ data, J. Geophys. Res.-Atmos., 122, 5870–5882, https://doi.org/10.1002/2016JD026282, 2017.

Condom, T., Martínez, R., Pabón, J. D., Costa, F., Pineda, L., Nieto, J. J., López, F., and Villacís, M.: Climatological and hydrological observations for the South American Andes: In situ stations, satellite, and reanalysis data sets, Front. Earth Sci., 8, 92, https://doi.org/10.3389/feart.2020.00092, 2020.

Davies, B., Gribbin, T., King, O., Matthews, T., Baiker, J. R., Becker, R., Buytaert, W., Carrivick, J., Drenkhan, F., García, J. L., Montoya, N., Perry, B., and Ely, J.: Landsystems of the tropical high Peruvian Andes: Glaciers, lakes, wetlands and water resources in the Cordillera Vilcanota, Earth Surf. Process. Landf., 51, e70296, https://doi.org/10.1002/esp.70296, 2026.

Emmer, A., Vilca, O., Salazar Checa, C., Li, S., Cook, S., Pummer, E., Hrebrina, J., and Haeberli, W.: Causes, consequences and implications of the 2023 landslide-induced Lake Rasac glacial lake outburst flood (GLOF), Cordillera Huayhuash, Peru, Nat. Hazards Earth Syst. Sci., 25, 1207–1228, https://doi.org/10.5194/nhess-25-1207-2025, 2025.

Espinoza, J. C., Chavez, S., Ronchail, J., Junquas, C., Takahashi, K., and Lavado, W.: Rainfall hotspots over the southern tropical Andes: Spatial distribution, rainfall intensity, and relations with large-scale atmospheric circulation, Water Resour. Res., 51, 3459–3475, https://doi.org/10.1002/2014WR016273, 2015.

Favier, V., Wagnon, P., Chazarin, J.-P., Maisincho, L., and Coudrain, A.: One-year measurements of surface heat budget on the ablation zone of Antizana Glacier 15, Ecuadorian Andes, J. Geophys. Res.-Atmos., 109, D18105, https://doi.org/10.1029/2003JD004359, 2004.

Ferreira, A. P., Azorin-Molina, C., and Gimeno, L.: Biases and uncertainties in radiosonde-based precipitable water vapor, Earth Space Sci., 13, e2026EA005075, https://doi.org/10.1029/2026EA005075, 2026.

Francou, B., Vuille, M., Wagnon, P., Mendoza, J., and Sicart, J.-E.: Tropical climate change recorded by a glacier in the central Andes during the last decades of the twentieth century: Chacaltaya, Bolivia, 16°S, J. Geophys. Res.-Atmos., 108, 4154, https://doi.org/10.1029/2002JD002959, 2003.

Garreaud, R., Vuille, M., and Clement, A. C.: The climate of the Altiplano: observed current conditions and mechanisms of past changes, Palaeogeogr. Palaeoclimatol. Palaeoecol., 194, 5–22, https://doi.org/10.1016/S0031-0182(03)00269-4, 2003.

Georges, C. and Kaser, G.: Ventilated and unventilated air temperature measurements for glacier-climate studies on a tropical high mountain site, J. Geophys. Res.-Atmos., 107, 4775, https://doi.org/10.1029/2002JD002503, 2002.

Goodison, B. E., Louie, P. Y. T., and Yang, D.: WMO solid precipitation measurement intercomparison: Final report, WMO

https://doi.org/10.5194/essd-2026-839
Preprint. Discussion started: 11 November 2026
© Author(s) 2026. CC BY 4.0 License.



`Instruments and Observing Method. 67, 212, 1998. https://library.wmo.int/idurl/4/28336

Gribbin, T., Mackay, J. D., MacDonald, A., Hannah, D. M., Buytaert, W., Baiker, J. R., Montoya, N., Perry, L. B., Seimon, A., Rado, M., Arias, S., and Vargas, M.: Bofedal wetland and glacial melt contributions to dry season streamflow in a high-Andean headwater watershed, Hydrol. Process., 38, e15237, https://doi.org/10.1002/hyp.15237, 2024.

Guy, H., Seimon, A., Perry, L. B., Konecky, B. L., Rado, M., Andrade, M., Potocki, M., and Mayewski, P. A.: Subseasonal variations of stable isotopes in tropical Andean precipitation, J. Hydrometeorol., 20, 915–933, https://doi.org/10.1175/JHM-D-18-0163.1, 2019.

Hardy, D. R., Vuille, M., Braun, C., Keimig, F., and Bradley, R. S.: Annual and daily meteorological cycles at high altitude on a tropical mountain, B. Am. Meteorol. Soc., 79, 1899–1914, https://doi.org/10.1175/1520-0477(1998)079%3C1899:AADMCA%3E2.0.CO;2, 1998.

Hersbach, H., Bell, B., Berrisford, P., Hirahara, S., Horányi, A., Muñoz-Sabater, J., Nicolas, J., Peubey, C., Radu, R., Schepers, D., Simmons, A., Soci, C., Abdalla, S., Abellan, X., Balsamo, G., Bechtold, P., Biavati, G., Bidlot, J., Bonavita, M., De Chiara, G., Dahlgren, P., Dee, D., Diamantakis, M., Dragani, R., Flemming, J., Forbes, R., Fuentes, M., Geer, A., Haimberger, L., Healy, S., Hogan, R. J., Hólm, E., Janisková, M., Keeley, S., Laloyaux, P., Lopez, P., Lupu, C., Radnoti, G., de Rosnay, P., Rozum, I., Vamborg, F., Villaume, S., and Thépaut, J.-N.: The ERA5 global reanalysis, Q. J. Roy. Meteor. Soc., 146, 1999–2049, https://doi.org/10.1002/qj.3803, 2020.

Holland, K. M., Criscitiello, A. S., McConnell, J. R., Markle, B. R., Yousif, H. A. K., Skelton, E., Wensman, S. M., Jensen, B. J. L., Winski, D. A., Campbell, S. W., and Chellman, N. J.: Unexpectedly high accumulation rates in the 2022 Mt. Logan ice core reveal warm-season drivers of precipitation variability, J. Geophys. Res.-Atmos., 131, e2025JD044951, https://doi.org/10.1029/2025JD044951, 2026.

Hurley, J. V., Vuille, M., Hardy, D. R., Burns, S. J., and Thompson, L. G.: Cold air incursions, $\delta^{18}O$ variability, and monsoon dynamics associated with snow days at Quelccaya Ice Cap, Peru, J. Geophys. Res.-Atmos., 120, 7467–7487, https://doi.org/10.1002/2015JD023323, 2015.

Hurley, J. V., Vuille, M., and Hardy, D. R.: On the interpretation of the ENSO signal embedded in the stable isotopic composition of Quelccaya Ice Cap, Peru, J. Geophys. Res.-Atmos., 124, 131–145, https://doi.org/10.1029/2018JD029064, 2019.

Hurst, D. F., Hall, E. G., Jordan, A. F., Miloshevich, L. M., Whiteman, D. N., Leblanc, T., Walsh, D., Vömel, H., and Oltmans, S. J.: Comparisons of temperature, pressure and humidity measurements by balloon-borne radiosondes and frost point hygrometers during MOHAVE-2009, Atmos. Meas. Tech., 4, 2777–2793, https://doi.org/10.5194/amt-4-2777-2011, 2011.

Immerzeel, W. W., Lutz, A. F., Andrade, M., Bahl, A., Biemans, H., Bolch, T., Hyde, S., Brumby, S., Davies, B. J., Elmore, A. C., Emmer, A., Feng, M., Fernández, A., Haritashya, U., Kargel, J. S., Koppes, M., Kraaijenbrink, P. D. A., Kulkarni, A. V., Mayewski, P. A., Nepal, S., Pacheco, P., Painter, T. H., Pellicciotti, F., Rajaram, H., Rupper, S., Sinisalo, A., Shrestha, A. B., Viviroli, D., Wada, Y., Xiao, C., Yao, T., and Baillie, J. E. M.: Importance and vulnerability of the world's

https://doi.org/10.5194/essd-2026-839
Preprint. Discussion started: 11 November 2026
© Author(s) 2026. CC BY 4.0 License.

water towers, Nature, 577, 364–369, https://doi.org/10.1038/s41586-019-1822-y, 2020.

Jonaitis, J. A., Perry, L. B., Soulé, P. T., Thaxton, C., Andrade-Flores, M. F., Vargas, T. I., and Ticona, L.: Spatiotemporal patterns of ENSO–precipitation relationships in the tropical Andes of southern Peru and Bolivia, Int. J. Climatol., 41, 4061–4076, https://doi.org/10.1002/joc.7058, 2021.

Junquas, C., Takahashi, K., Condom, T., Espinoza, J.-C., Chávez, S., Sicart, J.-E., and Lebel, T.: Understanding the influence of orography on the precipitation diurnal cycle and the associated atmospheric processes in the central Andes, Clim. Dynam., 50, 3995–4017, https://doi.org/10.1007/s00382-017-3858-8, 2018.

Kaser, G.: A review of the modern fluctuations of tropical glaciers, Global Planet. Change, 22, 93–103, https://doi.org/10.1016/S0921-8181(99)00028-4, 1999.

Khadka, A., Wagnon, P., Brun, F., Shrestha, D., Lejeune, Y., and Arnaud, Y.: Evaluation of ERA5-Land and HARv2 reanalysis data at high elevation in the upper Dudh Koshi basin (Everest region, Nepal), J. Appl. Meteorol. Clim., 61, 931–954, https://doi.org/10.1175/JAMC-D-21-0091.1, 2022.

Khadka, A., Perry, L. B., Matthews, T., Sherpa, T. G., Shrestha, C. B., Shrestha, D., Aryal, D., Tuladhar, S., Pradhananga, N., Kayastha, D., Raichle, B., Athans, P., Sherpa, D. Y., Garrett, K., Wheeler, G., Young, T., and Elmore, A.: Weather station data from the Mount Everest region, Nepal: 3810–8810 m above sea level, Earth Syst. Sci. Data, 18, 7253–7267, https://doi.org/10.5194/essd-18-7253-2026, 2026.

Khanal, S., Tiwari, S., Lutz, A. F., van den Hurk, B., and Immerzeel, W. W.: Historical climate trends over High Mountain Asia derived from ERA5 reanalysis data, J. Appl. Meteorol. Clim., 62, 263–288, https://doi.org/10.1175/JAMC-D-21-0045.1, 2023.

Kochendorfer, J., Nitu, R., Wolff, M., Mekis, E., Rasmussen, R., Baker, B., Earle, M. E., Reverdin, A., Wong, K., Smith, C. D., Yang, D., Roulet, Y.-A., Meyers, T., Buisan, S., Isaksen, K., Brækkan, R., Landolt, S., and Jachcik, A.: Testing and development of transfer functions for weighing precipitation gauges in WMO-SPICE, Hydrol. Earth Syst. Sci., 22, 1437–1452, https://doi.org/10.5194/hess-22-1437-2018, 2018.

Lamantia, K. A., Larocca, L. J., Thompson, L. G., and Mark, B. G.: El Niño enhances snow-line rise and ice loss on the Quelccaya Ice Cap, Peru, The Cryosphere, 18, 4633–4644, https://doi.org/10.5194/tc-18-4633-2024, 2024.

Matthews, T., Perry, L. B., Koch, I., Aryal, D., Khadka, A., Shrestha, D., Abernathy, K., Elmore, A. C., Seimon, A., Tait, A., Elvin, S., Tuladhar, S., Baidya, S. K., Potocki, M., Birkel, S. D., Kang, S., Sherpa, T. C., Gajurel, A., and Mayewski, P. A.: Going to extremes: Installing the world's highest weather stations on Mount Everest, B. Am. Meteorol. Soc., 101, E1870–E1890, https://doi.org/10.1175/BAMS-D-19-0198.1, 2020a.

Matthews, T., Perry, L. B., Lane, T. P., Elmore, A. C., Khadka, A., Aryal, D., Shrestha, D., Tuladhar, S., Baidya, S. K., Gajurel, A., Potocki, M., and Mayewski, P. A.: Into thick(er) air? Oxygen availability at humans' physiological frontier on Mount Everest, iScience, 23, 101718, https://doi.org/10.1016/j.isci.2020.101718, 2020b.

Musselman, K. N., Lehner, F., Ikeda, K., Clark, M. P., Prein, A. F., Liu, C., Barlage, M., and Rasmussen, R.: Projected increases and shifts in rain-on-snow flood risk over western North America, Nat. Clim. Change, 8, 808–812,

https://doi.org/10.5194/essd-2026-839
Preprint. Discussion started: 11 November 2026
© Author(s) 2026. CC BY 4.0 License.

https://doi.org/10.1038/s41558-018-0236-4, 2018.

Perez, N. and Loisel, J.: Synthesis of high-Andean peat cores reveals suite of Holocene climate conditions favorable for peat formation, Quaternary Sci. Rev., 322, 108413, https://doi.org/10.1016/j.quascirev.2023.108413, 2023.

Perry, L. B., Seimon, A., and Kelly, G. M.: Precipitation delivery in the tropical high Andes of southern Peru: new findings and paleoclimatic implications, Int. J. Climatol., 34, 197–215, https://doi.org/10.1002/joc.3679, 2014.

Perry, L. B., Seimon, A., Andrade-Flores, M. F., Endries, J. L., Yuter, S. E., Velarde, F., Arias, S., Bonshoms, M., Burton, E. J., Winkelmann, I. R., Cooper, C. M., Mamani, G., Rado, M., Montoya, N., and Quispe, N.: Characteristics of precipitating storms in glacierized tropical Andean cordilleras of Peru and Bolivia, Ann. Am. Assoc. Geogr., 107, 309–322, https://doi.org/10.1080/24694452.2016.1260439, 2017.

Perry, L. B., Matthews, T., Guy, H., Koch, I., Khadka, A., Elmore, A. C., Shrestha, D., Tuladhar, S., Baidya, S. K., Maharjan, S., Wagnon, P., Aryal, D., Seimon, A., Gajurel, A., and Mayewski, P. A.: Precipitation characteristics and moisture source regions on Mt. Everest in the Khumbu, Nepal, One Earth, 3, 594–607, https://doi.org/10.1016/j.oneear.2020.10.011, 2020.

Perry, L. B., Khadka, A., Cano, L., Seimon, A., Matthews, T., Arias, S., Guy, H., Montoya, N., Cooper, C., Rado, M., and Suarez, W. (2026). High-Elevation Meteorological Datasets from the Quelccaya Ice Cap and Surrounding Sites in the Cordillera Vilcanota, Peru [Dataset]. Zenodo. https://doi.org/10.5281/zenodo.23315967

Pitte, P., Perry, L. B., Matthews, T., Viale, M., Masiokas, M., Castro, M., Pecker Marcosig, I., Correas-Gonzalez, M., Cara, L., Jeanneret, P., Salas, M., Ghilardi, J. C., Guajardo, M., Ruiz, L., Wheeler, G., Cassella, V., Young, T., Garrett, K., Drake, S., Kochendorfer, J., Stein, A., and Elmore, A. C.: Wayra: an atmospheric observatory in the mid troposphere of the southern Andes, preprint, https://climatology.unr.edu/MET/Pitte_etal_2026_BAMS.pdf, 2026.

Poremba, R. J., Perry, L. B., Seimon, A., Martin, D. T., and Tupayachi, A.: Meteorological characteristics of heavy snowfall in the Cordillera Vilcanota, Peru, in: Proceedings of the 72nd Eastern Snow Conference, Sherbrooke, Québec, Canada, 9–11 June 2015, 167–180, https://climate.appstate.edu/~perrylb/Pubs/Proceedings/Poremba_etal_2015_ESC.pdf, 2015.

Pujol, O., Georgis, J.-F., Chong, M., and Roux, F.: Dynamics and microphysics of orographic precipitation during MAP IOP3, Q. J. Roy. Meteor. Soc., 131, 2795–2819, https://doi.org/10.1256/qj.04.79, 2005.

Rabatel, A., Francou, B., Soruco, A., Gomez, J., Cáceres, B., Ceballos, J. L., Basantes, R., Vuille, M., Sicart, J.-E., Huggel, C., Scheel, M., Lejeune, Y., Arnaud, Y., Collet, M., Condom, T., Consoli, G., Favier, V., Jomelli, V., Galarraga, R., Ginot, P., Maisincho, L., Mendoza, J., Ménégoz, M., Ramirez, E., Ribstein, P., Suarez, W., Villacis, M., and Wagnon, P.: Current state of glaciers in the tropical Andes: a multi-century perspective on glacier evolution and climate change, The Cryosphere, 7, 81–102, https://doi.org/10.5194/tc-7-81-2013, 2013.

Rasmussen, R., Baker, B., Kochendorfer, J., Meyers, T., Landolt, S., Fischer, A. P., Black, J., Thériault, J. M., Kucera, P., Gochis, D., Smith, C., Nitu, R., Hall, M., Ikeda, K., and Gutmann, E.: How well are we measuring snow? The NOAA/FAA/NCAR winter precipitation test bed, B. Am. Meteorol. Soc., 93, 811–829, https://doi.org/10.1175/BAMS-D-11-00052.1, 2012.

Richter, H.: How scientists unraveled the causes of the devastating flood in Tibet and Nepal, Science, 393, 954–955,

© Author(s) 2026. CC BY 4.0 License.



https://doi.org/10.1126/science.aem0437, 2026.

Roohi, M., Dehghani, J., Irani, M., and Mina, P.: A comprehensive review of flood damage in mountainous regions: challenges, solutions, and advanced management technologies, Discov. Geosci., 3, 59, https://doi.org/10.1007/s44288-025-00145-2, 2025.

Seimon, T. A., Seimon, A., Yager, K., Reider, K., Delgado, A., Sowell, P., Tupayachi, A., Konecky, B., McAloose, D., and Halloy, S.: Long-term monitoring of tropical alpine habitat change, Andean anurans, and chytrid fungus in the Cordillera Vilcanota, Peru: Results from a decade of study, Ecol. Evol., 7, 1527–1540, https://doi.org/10.1002/ece3.2779, 2017.

Sierra, J. P., Junquas, C., Espinoza, J. C., Segura, H., Condom, T., Andrade, M., Molina-Carpio, J., Ticona, L., Mardoñez, V., Blacutt, L., Polcher, J., Rabatel, A., and Sicart, J. E.: Deforestation impacts on Amazon-Andes hydroclimatic connectivity, Clim. Dynam., 58, 2609–2636, https://doi.org/10.1007/s00382-021-06025-y, 2022.

Thompson, L. G., Hastenrath, S., and Morales Arnao, B.: Climatic ice core records from the tropical Quelccaya ice cap, Science, 203, 1240–1243, https://doi.org/10.1126/science.203.4386.1240, 1979.

Thompson, L. G., Mosley-Thompson, E., Bolzan, J. F., and Koci, B. R.: A 1500-year record of tropical precipitation in ice cores from the Quelccaya ice cap, Peru, Science, 229, 971–973, https://doi.org/10.1126/science.229.4717.971, 1985.

Thompson, L. G., Mosley-Thompson, E., Davis, M. E., Zagorodnov, V. S., Howat, I. M., Mikhalenko, V. N., and Lin, P.-N.: Annually resolved ice core records of tropical climate variability over the past ~1800 years, Science, 340, 945–950, https://doi.org/10.1126/science.1234210, 2013.

Thompson, L. G., Davis, M. E., Mosley-Thompson, E., Beaudon, E., Porter, S. E., Kutuzov, S., Lin, P.-N., Mikhalenko, V. N., and Mountain, K. R.: Impacts of recent warming and the 2015/2016 El Niño on tropical Peruvian ice fields, J. Geophys. Res.-Atmos., 122, 12688–12701, https://doi.org/10.1002/2017JD026592, 2017.

Thompson, L. G., Davis, M. E., Mosley-Thompson, E., Porter, S. E., Valdivia Corrales, G., Shuman, C. A., and Tucker, C. J.: The impacts of warming on rapidly retreating high-altitude, low-latitude glaciers and ice core-derived climate records, Global Planet. Change, 203, 103538, https://doi.org/10.1016/j.gloplacha.2021.103538, 2021.

Turpo Cayo, E. Y., Borja, M. O., Espinoza-Villar, R., Moreno, N., Camargo, R., Almeida, C., Hopfgartner, K., Yarleque, C., and Souza, C. M., Jr.: Mapping three decades of changes in the tropical Andean glaciers using Landsat data processed in the Earth Engine, Remote Sens., 14, 1974, https://doi.org/10.3390/rs14091974, 2022.

Wagnon, P., Sicart, J.-E., Berthier, E., and Chazarin, J.-P.: Wintertime high-altitude surface energy balance of a Bolivian glacier, Illimani, 6340 m above sea level, J. Geophys. Res.-Atmos., 108, 4177, https://doi.org/10.1029/2002JD002088, 2003.

Yarleque, C., Vuille, M., Hardy, D. R., Elison Timm, O., De la Cruz, J., Ramos, H., and Rabatel, A.: Projections of the future disappearance of the Quelccaya Ice Cap in the Central Andes, Sci. Rep., 8, 15564, https://doi.org/10.1038/s41598-018-33698-z, 2018.

Zou, C., Jansen, J. D., Dou, X., Dai, L., Xu, Q., and Fan, X.: Elevation-dependent landsliding driven by climate change in the eastern Himalayan syntaxis, Natl. Sci. Rev., 13, nwag238, https://doi.org/10.1093/nsr/nwag238, 2026.